

# Numerical computation of capillary–gravity interfacial solitary waves

By O. LAGET<sup>1,2</sup> AND F. DIAS<sup>1</sup>

<sup>1</sup>Institut Non-Linéaire de Nice, UMR 6618 – CNRS & UNSA, 1361 route des Lucioles,  
F-06560 Valbonne, France

<sup>2</sup>Principia Recherche et Développements, Z. I. de Brégaillon, F-83507 La Seyne sur mer, France

(Received 10 February 1997 and in revised form 28 April 1997)

Two types of capillary–gravity interfacial solitary waves are computed numerically: ‘classical’ solitary waves which bifurcate from a uniform flow at a critical value of the velocity and solitary waves in the form of wave packets which bifurcate from a train of infinitesimal periodic waves with equal phase and group velocities. The effects of finite amplitude are shown to be quite different from the pure gravity case for the classical solitary waves. The solitary waves in the form of wave packets, which are known to exist for small density ratios, are shown to exist even for larger density ratios, but only at finite amplitude. The numerical code is based on an integro-differential formulation of the full Euler equations. The experimental results of Koop & Butler (1981), which have been compared earlier with results from model equations, are compared with the present numerical results.

---

## 1. Introduction

Solitary waves that propagate steadily along the interface between two fluids, with a lighter fluid lying above a heavier one, are studied. Both gravity and capillary–gravity waves are considered.

In the case where the fluids occupy a closed channel of infinite horizontal and constant uniform vertical extent, i.e. in the so-called rigid-lid configuration, it is well known that gravity solitary waves bifurcate from a uniform flow at a critical value of the fluids velocity  $c$  given by

$$c^2 = gh_1 \left( \frac{1 - R}{1 + R/H} \right), \quad (1.1)$$

where  $h_1$  denotes the depth of the lower layer,  $g$  the acceleration due to gravity,  $R$  the ratio of densities and  $H$  the ratio of fluid depths  $h_2/h_1$ . The speed of the bifurcated waves is larger than  $c$ . Such waves have been studied experimentally by Koop & Butler (1981) and by Michallet & Barthélémy (1996) for example. Considering either true solitary waves or periodic waves of very long wavelength, Funakoshi & Oikawa (1986), Turner & Vanden-Broeck (1988), Pullin & Grimshaw (1988), Mirie & Pennell (1989), Sha & Vanden-Broeck (1993), Moni & King (1995) and Evans & Ford (1996) followed numerically the solitary waves away from the bifurcation point by increasing the velocity.

Whether the bifurcating solitary waves are of elevation or depression depends on the sign of  $H^2 - R$ . If  $H^2 - R > 0$ , the waves are of elevation. If  $H^2 - R < 0$ , the waves are of depression. Several studies have been devoted to the particular case where

$H^2 \approx R$ . Amick & Turner (1989) and Mielke (1995) provided a proof of existence of small-amplitude fronts.

The effects of surface tension on the interfacial solitary waves described above have been studied by Kirrmann (1991). As for surface waves, there are also capillary-gravity solitary waves bifurcating from a uniform flow when the speed is equal to the value given by (1.1). However, if the Weber number

$$W = \frac{\sigma}{\rho_1(h_1 + h_2)c^2},$$

where  $\sigma$  is the coefficient of interfacial tension and  $\rho_1$  the density of the lower fluid, is non-zero and less than a critical value

$$W^* = \frac{1}{3} \left( \frac{1 + RH}{1 + H} \right),$$

the solitary waves are generalized, in the sense that they have ripples in their tail. These ripples are periodic waves whose phase velocity is the same as the speed of the solitary wave. For high enough surface tension ( $W > W^*$ ), the solitary waves are true solitary waves as in the gravity case. However, the dependence on the sign of  $H^2 - R$  is exactly the opposite. The solitary waves are of elevation if  $H^2 - R < 0$  and of depression if  $H^2 - R > 0$ . Kirrmann (1991) performed an analysis near the critical case where  $H^2 \approx R$  and found among all possible solutions solitary waves with an algebraic decay towards infinity. Kirrmann's analysis is a weakly nonlinear analysis valid near the bifurcation point (1.1). One of the goals of this paper is to provide numerical results based on the full Euler equations for these 'classical' capillary-gravity solitary waves when the Weber number is sufficiently large ( $W > W^*$ ). Exponentially decaying as well as algebraically decaying solitary waves will be considered.

All the work described above focuses on solitary waves bifurcating from infinitesimal long waves. Such waves bifurcate when the phase speed  $c$  is equal to the value corresponding to the local extremum of the dispersion relation  $c(k)$  at  $k = 0$ , where  $k$  denotes the wavenumber. More recently, attention has been given to the case where the phase speed  $c$  is equal to the value corresponding to the minimum of the dispersion relation at  $k = k^*$ , with  $k^* \neq 0$ , when such a minimum exists. This case was first considered for surface waves in finite depth by Iooss & Kirchgässner (1990) and extended to infinite depth by Iooss & Kirrmann (1996). In both cases, the existence of symmetric solitary waves in the form of wave packets with damped oscillations in their tail, bifurcating from infinitesimal periodic waves with  $k = k^*$ , was proved. In finite depth, the envelope decays exponentially towards infinity while in infinite depth the decay is algebraic. The results were partially extended to interfacial waves by Dias & Iooss (1994), (1996) for the full Euler equations, and by Benjamin (1992), (1996) for a model equation. Another goal of this paper is to provide numerical results based on the full Euler equations for these capillary-gravity solitary waves in the form of wave packets. The computations will be restricted to infinite depth.

In §2, the mathematical formulation of the problem is provided. Section 3 is devoted to 'classical' solitary waves, while §4 is devoted to solitary waves in the form of wave packets. Sections 3 and 4 follow the same structure: the linear as well as the nonlinear analytical results are described first. Then the numerical scheme used to solve the problem is presented. Then various model equations and their solutions are reviewed or obtained. Finally numerical results are presented. The last section (§5) discusses the limiting configurations of interfacial solitary waves, some of their properties as well as the physical relevance of the computed solutions and their stability. Appendix

Symbol	Physical quantity	Dimension
$c$	wave velocity	$[L][T]^{-1}$
$\sigma$	coefficient of interfacial tension	$[M][T]^{-2}$
$g$	acceleration due to gravity	$[L][T]^{-2}$
$h_j$	depth of the layer $j$	$[L]$
$\rho_j$	density of the fluid in the layer $j$	$[M][L]^{-3}$
$k$	wave number	$[L]^{-1}$
$(x, y)$	physical coordinates	$[L]$
$(u_j, v_j)$	velocity components in layer $j$	$[L][T]^{-1}$
$\psi_j(x, y)$	stream function $\psi_{jx} = -v_j, \psi_{jy} = u_j$	$[L]^2[T]^{-1}$
$\phi_j(x, y)$	velocity potential $\phi_{jx} = u_j, \phi_{jy} = v_j$	$[L]^2[T]^{-1}$
$\eta(x)$	profile of the interface	$[L]$

TABLE 1. Physical parameters and their dimension

Symbol	Definition	Dimensionless quantity
$K$	$k(h_1 + h_2)$	dimensionless wavenumber
$H$	$h_2/h_1$	depth ratio
$H_j$	$h_j/(h_1 + h_2)$	relative depth of layer $j$
$R$	$\rho_2/\rho_1$	density ratio
$W$	$\sigma/[\rho_1(h_1 + h_2)c^2]$	Weber number
$F^2$	$c^2/[(1 - R)g(h_1 + h_2)]$	square of Froude number
$X$	$x/(h_1 + h_2)$	dimensionless horizontal coordinate
$Y(X)$	$\eta/(h_1 + h_2)$	dimensionless profile of the interface
$(\Phi_j, \Psi_j)$	$1/[c(h_1 + h_2)](\phi_j, \psi_j)$	dimensionless potential and stream function

TABLE 2. Dimensionless quantities

A provides a straightforward description of conjugate flows. Appendix B describes the reduction method used to obtain the model equations.

### 2. Formulation

The problem is formulated in a frame of reference moving with the solitary wave. Therefore, the velocity in both fluids approaches  $c$  at infinity. All quantities related to the upper fluid layer have the index 2, while those related to the lower layer are indexed with 1. All the physical parameters as well as the dimensionless numbers are provided in tables 1 and 2. The  $x$ -axis coincides with the interface at rest. The  $y$ -axis is vertical.

The continuity equation and the irrotationality condition can be written in each layer in the form

$$\left. \begin{aligned} u_{ix} + v_{iy} &= 0 \\ u_{iy} - v_{ix} &= 0 \end{aligned} \right\} \quad i = 1, 2. \tag{2.1}$$

The boundary conditions along the walls are

$$v_1(x, -h_1) = 0, \tag{2.2}$$

$$v_2(x, h_2) = 0. \tag{2.3}$$

At the interface, there are two kinematic conditions

$$u_i \eta_x - v_i = 0, \quad i = 1, 2, \quad \text{at } y = \eta(x). \tag{2.4}$$

Using Bernoulli's equation in each fluid and eliminating the pressures at the interface,

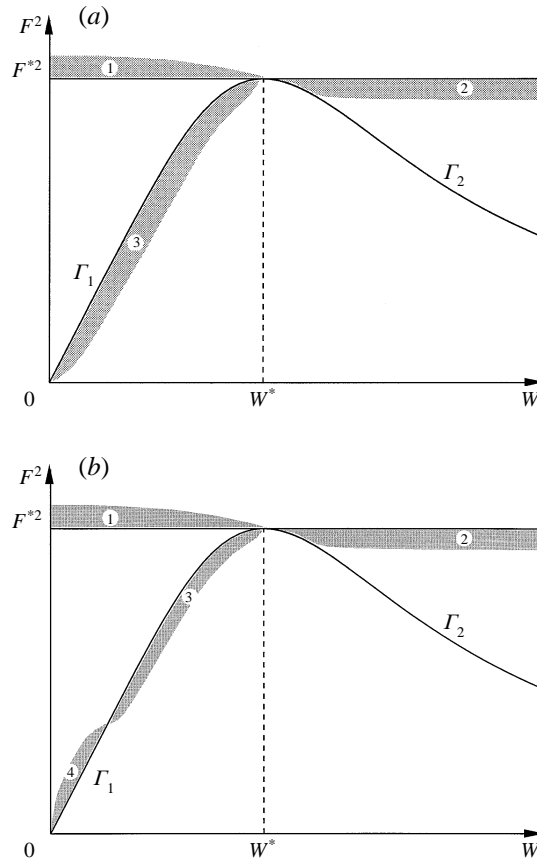


FIGURE 1. The shaded regions indicate values of the parameters  $F$  and  $W$  where small-amplitude solitary waves are known to exist. In region 1, there are generalized solitary waves (with non-decaying oscillations in their tail), which bifurcate from a uniform flow with speed  $F^*$  (3.1). These waves are not considered in this paper. In the limit  $W \rightarrow 0$ , these generalized solitary waves become the well-known classical gravity solitary waves which have been studied in several papers. In region 2, there are capillary-gravity solitary waves, which also bifurcate from a uniform flow with speed  $F^*$  (3.1). These waves are considered in § 3. In region 3, there are true capillary-gravity solitary waves in the form of wave packets. They bifurcate along the curve  $\Gamma_1$  which is given in parametric form in § 4.1. These waves are considered in § 4. The diagrams (a) and (b) are drawn for some given values of  $R$  and  $H$ . They do not change qualitatively as  $H$  varies. However, as  $R$  varies, the bifurcations along the curve  $\Gamma_1$  change. For small enough values of  $R$ , the bifurcations are qualitatively similar to the free-surface problem (a). For large enough values of  $R$ , (b), there are also generalized solitary waves in region 4. These waves are not considered in this paper. The curve  $\Gamma_2$  is discussed in § 3.

one can write the dynamic condition in the form

$$\frac{1}{2}\rho_1(u_1^2 + v_1^2) - \frac{1}{2}\rho_2(u_2^2 + v_2^2) + (\rho_1 - \rho_2)g\eta - \frac{\sigma\eta_{xx}}{(1 + \eta_x^2)^{3/2}} = \frac{1}{2}(\rho_1 - \rho_2)c^2 \quad \text{at } y = \eta(x). \quad (2.5)$$

The dispersion relation for linearized interfacial waves is given by

$$D(F, W, R, H; K) = 0,$$

where

$$D(F, W, R, H; K) \equiv (F^{-2} + WK^2) \tanh(KH_1) \tanh(KH_2) - K [R \tanh(KH_1) + \tanh(KH_2)]. \quad (2.6)$$

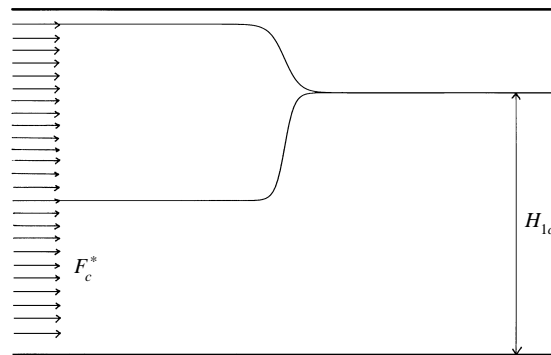


FIGURE 2. Properties of conjugate flows. In both cases, the upstream velocity is the same, equal to  $F = F_c^* \equiv (1 + R^{1/2})^{-1}$ . In both cases, the interface is at the same level downstream. The value of  $H_1$  is  $H_{1c} \equiv (1 + R^{1/2})^{-1}$ . The profiles of the fronts have not been computed on the full equations but on the modified Korteweg–de Vries equation (A 20).

The problem involves four parameters: the Froude number  $F$ , the Weber number  $W$ , the density ratio  $R$  and the depth ratio  $H$ . However, the bifurcation diagram depends only on  $F$  and  $W$ , at least qualitatively. For most values of  $R$  and  $H$ , the bifurcation diagram in the  $(W, F^2)$ -plane for the two-fluid system is qualitatively similar to that for the free-surface problem of a single layer of fluid of finite height (see figure 1a). The generalized solitary waves bifurcate along the line  $F = F^*$  with  $0 < W < W^*$  (region 1), the ‘classical’ solitary waves bifurcate along the line  $F = F^*$  with  $W = 0$  or  $W > W^*$  (region 2), the solitary waves in the form of wave packets bifurcate along the curve  $\Gamma_1$  (region 3). Note however that for large enough values of  $R$  the picture changes slightly along the curve  $\Gamma_1$  (see figure 1b). It is possible to have a region 4 where dark solitary waves are present. Dark solitary waves approach the same periodic wave with a phase shift at  $+\infty$  and  $-\infty$ . The curve  $\Gamma_2$  will be discussed in § 3.

### 3. ‘Classical’ solitary waves

#### 3.1. Linear results

The Taylor expansion of (2.6) near  $K = 0$  starts with the  $K^2$  term and contains only even powers of  $K$ . It is easy to show that the coefficient of  $K^2$  vanishes when  $F = F^*$ , and that in addition the coefficient of  $K^4$  vanishes as well when  $W = W^*$ , where the critical values  $F^*$  and  $W^*$  are given by

$$\frac{1}{F^{*2}} = \frac{1}{H_1} + \frac{R}{H_2}, \quad W^* = \frac{1}{3} (H_1 + RH_2). \tag{3.1}$$

In other words, we have  $D(F^*, W, R, H; K) = O(K^4)$  and  $D(F^*, W^*, R, H; K) = O(K^6)$  for  $K \rightarrow 0$ . For  $R = 0$  and  $H_1 = 1$ , which corresponds to the free-surface problem, we recover the well-known values  $F^* = 1$  and  $W^* = \frac{1}{3}$ .

#### 3.2. Nonlinear results

In the region  $F$  near  $F^*$ , solutions are similar to those of the free-surface problem if  $H^2 > R$  (elevation gravity solitary waves, depression capillary–gravity solitary waves), while they differ if  $H^2 < R$  (depression gravity solitary waves, elevation capillary–gravity solitary waves). When  $H^2 \approx R$  and  $W = 0$ , there are gravity fronts (see figure

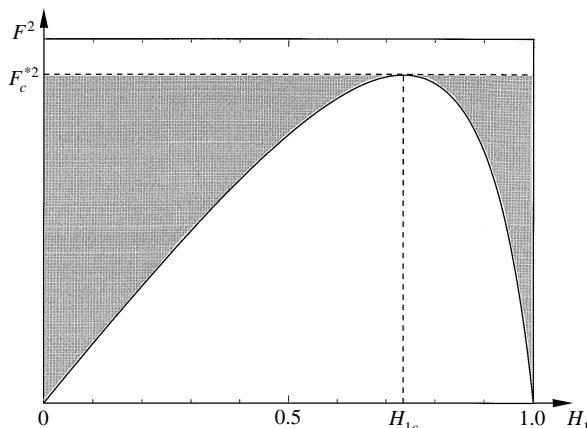


FIGURE 3. Types of solutions in the plane  $F^2$  versus  $H_1$  for  $R = 0.13$  and  $W = 0$ . The curve corresponds to (3.1). The horizontal dotted line corresponds to (3.2). The upstream Froude number for all fronts is equal to  $F_c^*$ . Solitary waves are present in the shaded regions. They bifurcate along the curve. They are of elevation if  $H_1 < H_{1c}$  and of depression if  $H_1 > H_{1c}$ . For a fixed value of  $H_1$  not too far from  $H_{1c}$  the amplitude of the solitary wave increases and the wave broadens as  $F$  increases, until  $F$  reaches the line  $F = F_c^*$  where the broadening is 'infinite'.

2). The properties of these fronts can be obtained by writing the conservation of mass, momentum and energy (see Appendix A). The upstream speed is always

$$c^2 = g(h_1 + h_2) \frac{1 - R^{1/2}}{1 + R^{1/2}} \quad \text{or} \quad F = \frac{1}{1 + R^{1/2}}, \quad (3.2)$$

while the amplitude is

$$H_1 = H_{1c} \equiv \frac{1}{1 + R^{1/2}}. \quad (3.3)$$

These properties are illustrated in figure 2. The profiles, which have been computed using the model equation which will be introduced in § 3.4.2, are given by (A 21).

Note also that the maximum of the curve (3.1) giving the critical Froude number  $F^*$  as a function of  $H_1$ ,

$$F^{*2}(H_1) = \frac{H_1(1 - H_1)}{1 - (1 - R)H_1},$$

is reached precisely when  $H_1 = H_{1c}$ , i.e.  $H^2 = R$ . We denote  $F^*(H_{1c})$  by  $F_c^*$ .

The results which are known for gravity waves are summarized in figure 3. The curve represents  $F^{*2}(H_1)$ . Solitary waves exist inside the shaded regions. The waves are of elevation if  $H_1 < H_{1c}$  and of depression if  $H_1 > H_{1c}$ . Solitary waves bifurcate from a uniform flow along the curve. As  $F$  increases with  $H_1$  fixed, the amplitude of the solitary wave increases. At the same time, the wave broadens. As  $F$  approaches  $F_c^*$ , the broadening becomes infinite. This is known to be true if  $H_1$  is not too far from  $H_{1c}$ . For values of  $H_1$  close to 0 or to 1, the fate of the solitary waves as  $F$  approaches  $F_c^*$  still is an open problem. Therefore, it is not known yet whether the shaded regions occupy the whole regions between the curve and the line  $F = F_c^*$ . We tried to explore this problem with our code but we were not able to draw conclusions because of a lack of precision. This problem is discussed again in § 5.

For capillary-gravity waves,  $R = H^2$  is also a singularity but the consequences are different. We will show in § 3.5 that solitary waves occupy the region inside the curve

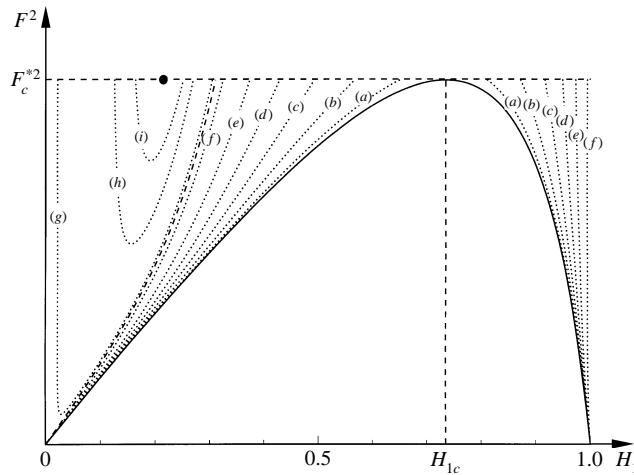


FIGURE 4. Decay rate of gravity solitary waves at infinity. For  $R = 0.13$ , we picked several values for  $\kappa$  in (3.4) ( $\kappa = 0.5$  (a), 1 (b), 1.5 (c), 2 (d), 2.5 (e), 3 (f), 3.2 (g), 3.5 (h), 3.6 (i)) and computed the corresponding values of  $F^2(H_1)$ . The dashed line corresponds to  $\kappa = \pi$ . The big dot represents the maximum decay rate  $\kappa = 3.67$ , which is obtained for  $F = F_c^*$ ,  $H_1 = 0.214$ .

and that for a fixed value of  $F$  branches connect one side of the curve to the other. At the end point opposite to the bifurcation point, the decay of the solitary wave is algebraic.

The dispersion relation (2.6) provides the decay rate at infinity of solitary waves. Set  $K = i\kappa$  in (2.6). The real number  $\kappa$  is solution of the equation

$$\frac{1}{F^2} - W \kappa^2 = \kappa \left[ \frac{R}{\tan(\kappa H_2)} + \frac{1}{\tan(\kappa H_1)} \right]. \tag{3.4}$$

For fixed values of the parameters  $F$ ,  $W$ ,  $R$  and  $H$ , this equation admits an infinity of solutions. The decay rate is given by the smallest root. Solutions of (3.4) are represented in figure 4 for gravity waves ( $W = 0$ ). Results for capillary–gravity waves will be given in § 3.5.

### 3.3. Numerical scheme

The scheme is exactly the same as the one used by Dias, Menasce & Vanden-Broeck (1996) in the free-surface case, except that it is extended to two fluids. The interfacial-wave problem is solved numerically by a boundary integral equation technique. The complex potentials  $\Phi_j + i\Psi_j$  are introduced and chosen as the independent variables. Without loss of generality, we choose  $\Psi = 0$  on the interface and  $\Phi_j = 0$  at  $X = 0$ .

The values of  $X$  and  $Y$  on the interface  $\Psi = 0$  are denoted by  $X_j(\Phi_j)$  and  $Y_j(\Phi_j)$ . By using Cauchy’s integral formula, one can obtain integro-differential equations for  $X'_j(\Phi_j)$  and  $Y'_j(\Phi_j)$ , where the primes denote differentiation with respect to  $\Phi_j$ . Let the link between both potentials be given by

$$\Phi_2 = g(\Phi_1).$$

Of course

$$X_1(\Phi_1) = X_2(\Phi_2), \quad Y_1(\Phi_1) = Y_2(\Phi_2).$$

At infinity, the asymptotic behaviour of the potentials is

$$\frac{dX}{d\Phi_1} \rightarrow 1, \quad \frac{dX}{d\Phi_2} \rightarrow 1, \quad \text{and therefore} \quad \frac{d\Phi_2}{d\Phi_1} \rightarrow 1.$$

The equations obtained from Cauchy's formula are

$$\begin{aligned} X'_1 &= 1 - \frac{1}{\pi} \int_0^{+\infty} Y'_1 \left( \frac{1}{s - \Phi_1} + \frac{1}{s + \Phi_1} \right) ds \\ &\quad + \frac{1}{\pi} \int_0^{+\infty} \frac{-(s - \Phi_1)Y'_1 + 2H_1(X'_1 - 1)}{(s - \Phi_1)^2 + 4H_1^2} ds \\ &\quad + \frac{1}{\pi} \int_0^{+\infty} \frac{-(s + \Phi_1)Y'_1 + 2H_1(X'_1 - 1)}{(s + \Phi_1)^2 + 4H_1^2} ds, \end{aligned} \quad (3.5)$$

and

$$\begin{aligned} \frac{X'_1}{g'} &= 1 + \frac{1}{\pi} \int_0^{+\infty} Y'_1 \left( \frac{1}{g(s) - g(\Phi_1)} + \frac{1}{g(s) + g(\Phi_1)} \right) ds \\ &\quad + \frac{1}{\pi} \int_0^{+\infty} \frac{[g(s) - g(\Phi_1)]Y'_1 + 2H_2(X'_1 - g')}{[g(s) - g(\Phi_1)]^2 + 4H_2^2} ds \\ &\quad + \frac{1}{\pi} \int_0^{+\infty} \frac{[g(s) + g(\Phi_1)]Y'_1 + 2H_2(X'_1 - g')}{[g(s) + g(\Phi_1)]^2 + 4H_2^2} ds. \end{aligned} \quad (3.6)$$

Bernoulli's equation is

$$\frac{1}{2} \left( \frac{1}{X_1'^2 + Y_1'^2} \right) (1 - Rg'^2) + \frac{1}{F^2} Y_1 + W \frac{Y_1' X_1'' - X_1' Y_1''}{(X_1'^2 + Y_1'^2)^{3/2}} = \frac{1}{2}(1 - R). \quad (3.7)$$

The three equations (3.5), (3.6), (3.7) must be solved for the three unknowns  $Y_1$ ,  $g$  and  $X_1$ . The system is discretized by choosing  $N$  points for the potential  $\Phi_1$  with an equal spacing  $\Delta\Phi$  and solved by Newton's method for fixed values of the parameters  $R$ ,  $F$ ,  $W$ ,  $H$ . The Cauchy principal values are evaluated by using mid-points for the integrations.

### 3.4. Analytical solutions

In order to follow the branches of solutions, we start near the bifurcation curves where a good initial guess is provided by the analytical solutions.

We give the expressions for the steady Korteweg–de Vries equation, the higher-order Korteweg–de Vries equation as well as the modified Korteweg–de Vries equation, which are valid in certain regions of parameter space. Such equations have already been provided by Sun & Shen (1993). An alternative derivation using centre-manifold reduction and normal forms is provided in Appendix B.

#### 3.4.1. Korteweg–de Vries equation

When  $F$  is close to  $F^*$ ,  $R$  not too close to  $H^2$  and  $W$  either equal to 0 or larger than  $W^*$  (but not too close to  $W^*$ ), the full equations can be reduced to the Korteweg–de Vries equation which, integrated once, can be written as

$$\mu Y + (W^* - W)Y_{XX} + \frac{3}{2H_1^2} \left( 1 - \frac{R}{H^2} \right) Y^2 = 0, \quad (3.8)$$



where  $\mu$  is the bifurcation parameter defined by

$$\mu = \frac{1}{F^2} - \frac{1}{F^{*2}}.$$

Recall that  $\mu < 0$  for gravity waves and  $\mu > 0$  for capillary-gravity waves. If  $\mu > 0$ , one can introduce the change of variables

$$\mu \tilde{Y} = Y, \quad \tilde{X} = \mu^{1/2} (W - W^*)^{-1/2} X,$$

and define the elevation number  $E$  as

$$E = -\frac{3}{2H_1^2} \left( 1 - \frac{R}{H^2} \right).$$

The resulting equation is

$$\tilde{Y} - \tilde{Y}_{\tilde{X}\tilde{X}} - E\tilde{Y}^2 = 0, \tag{3.9}$$

which admits solitary wave solutions of the form

$$\tilde{Y} = \frac{3}{2E \cosh^2 \left( \frac{1}{2} \tilde{X} \right)}. \tag{3.10}$$

When  $E > 0$ , i.e.  $H^2 < R$ , the waves are of elevation. When  $E < 0$ , i.e.  $H^2 > R$ , the waves are of depression.

### 3.4.2. Modified Korteweg-de Vries equation

The unfolding of the singularity  $H^2 = R$  leads to the modified Korteweg-de Vries equation

$$\mu Y + (W_c^* - W)Y_{XX} + \frac{3}{2H_{1c}^2} \left( 1 - \frac{R}{H^2} \right) Y^2 - \frac{2}{H_{1c}^4 H_c} Y^3 = 0. \tag{3.11}$$

Recall that  $H_{1c} = (1 + R^{1/2})^{-1}$  and  $W_c^* = W^*(H_{1c})$ .

If  $\mu = 0$ , there is a non-trivial solitary wave solution, with algebraic decay at infinity, given by

$$Y = \frac{4H_{1c}H_{2c}(W - W_c^*)(1 - R/H^2)}{H_c(1 - R/H^2)^2 X^2 + 4(W - W_c^*)}. \tag{3.12}$$

This solitary wave is of elevation if  $H^2 > R$  and of depression if  $H^2 < R$ .

If  $\mu \neq 0$ , one can introduce the change of variables

$$\mu^{1/2} \tilde{Y} = \frac{1}{H_{1c}^2} \left( \frac{2}{H_c} \right)^{1/2} Y, \quad \tilde{X} = \mu^{1/2} (W - W_c^*)^{-1/2} X,$$

and define the coefficient  $Q$  as

$$Q = -\frac{3}{2} \left( \frac{H_c}{2\mu} \right)^{1/2} \left( 1 - \frac{R}{H^2} \right).$$

The resulting equation is

$$\tilde{Y} - \tilde{Y}_{\tilde{X}\tilde{X}} - Q\tilde{Y}^2 - \tilde{Y}^3 = 0, \tag{3.13}$$

which is valid if the difference  $|H^2 - R|$  is of the order of  $\mu^{1/2}$ . This equation admits

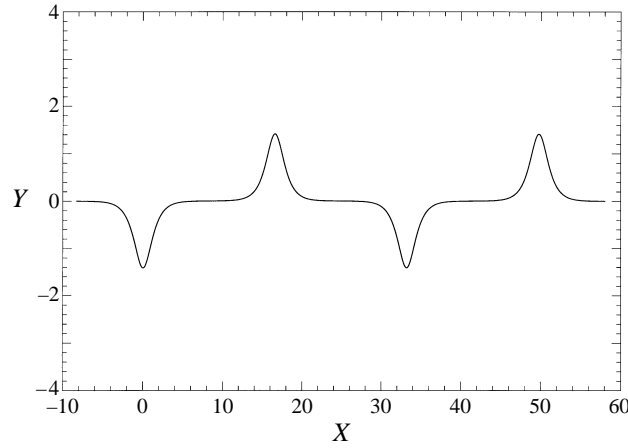


FIGURE 5. A periodic solution of the modified Korteweg–de Vries equation (3.11), which is a succession of humps and hollows.

solitary wave solutions of elevation as well as of depression:

$$\tilde{Y} = \frac{3}{Q} \frac{1}{(1 + 9/2Q^2)^{1/2} [\cosh^2(\frac{1}{2}\tilde{X}) + \sinh^2(\frac{1}{2}\tilde{X})] + 1}, \quad (3.14)$$

$$\tilde{Y} = -\frac{3}{Q} \frac{1}{(1 + 9/2Q^2)^{1/2} [\cosh^2(\frac{1}{2}\tilde{X}) + \sinh^2(\frac{1}{2}\tilde{X})] - 1}. \quad (3.15)$$

When  $Q = 0$ , (3.14)–(3.15) become

$$\tilde{Y} = \pm \frac{\sqrt{2}}{\cosh^2(\frac{1}{2}\tilde{X}) + \sinh^2(\frac{1}{2}\tilde{X})}. \quad (3.16)$$

The new feature for capillary–gravity solitary waves as opposed to gravity solitary waves is that depression and elevation waves can coexist.

Although the emphasis of this paper is on solitary waves and not on periodic waves, it is interesting to consider the periodic waves of (3.11) when they are close to the limit of the solitary waves (3.14) and (3.15). They look like a succession of humps and hollows. Figure 5 shows a periodic solution of the modified Korteweg–de Vries equation (3.11).

### 3.4.3. Fifth-order Korteweg–de Vries equation

The unfolding of the singularity  $W = W^*$  leads to the higher-order Korteweg–de Vries equation

$$\mu Y + (W^* - W)Y_{XX} + \frac{1}{45}(H_1^3 + RH_2^3)Y_{XXXX} + \frac{3}{2H_1^2} \left(1 - \frac{R}{H^2}\right) Y^2 = 0. \quad (3.17)$$

One can introduce the change of variables

$$\mu \tilde{Y} = Y, \quad \tilde{X} = \mu^{1/4} \left( \frac{45}{H_1^3 + RH_2^3} \right)^{1/4} X,$$

and define the coefficients  $Q$  and  $\tau$  as

$$Q = -\frac{3}{2H_1^2} \left(1 - \frac{R}{H^2}\right), \quad \tau = \frac{1}{\mu^{1/2}} \left(\frac{45}{H_1^3 + RH_2^3}\right)^{1/2} (W - W^*).$$

The resulting equation is

$$\tilde{Y} - \tau \tilde{Y}_{\tilde{X}\tilde{X}} + \tilde{Y}_{\tilde{X}\tilde{X}\tilde{X}\tilde{X}} - Q\tilde{Y}^2 = 0.$$

No general explicit solution of this equation is known. However, when  $\tau = 13/6$ , there is an explicit solution given by

$$\tilde{Y} = \frac{35}{24} \frac{1}{Q \cosh^4\left(\frac{1}{12}\tilde{X}\sqrt{6}\right)}.$$

This wave is of elevation if  $H^2 < R$  and of depression if  $H^2 > R$ .

### 3.4.4. Modified fifth-order Korteweg-de Vries equation

Near the codimension-3 singularity  $F = F^*, W = W^*, H = R^2$ , one could in principle write a higher-order modified Korteweg-de Vries equation

$$\mu Y + (W^* - W)Y_{XX} + \frac{1}{45}(H_{1c}^3 + RH_{2c}^3)Y_{XXXX} + \frac{3}{2H_{1c}^2} \left(1 - \frac{R}{H^2}\right) Y^2 - \frac{2}{H_{1c}^3 H_{2c}} Y^3 = 0. \tag{3.18}$$

We will not say anything more on (3.18). However, in §5, we will show that the conditions for this codimension-3 singularity might be obtained experimentally.

### 3.5. Numerical results

Computations were performed using the numerical scheme described in §3.3, for various values of the Froude number  $F$ , the Weber number  $W$ , the ratio of densities  $R$  and the ratio of heights  $H$ .

The case  $W = 0$  corresponds to gravity solitary waves. As said in the Introduction, these waves have been computed by several researchers. However, to our knowledge, computations based on the full equations have never been used for comparison with the experimental results of Koop & Butler (1981). These results have been compared with the results provided by the Korteweg-de Vries (KdV) equation. The Korteweg-de Vries equation for gravity waves is

$$-\mu Y + W^* Y_{XX} + \frac{3}{2H_1^2} \left(1 - \frac{R}{H^2}\right) Y^2 = 0, \tag{3.19}$$

where  $\mu$  is the bifurcation parameter defined by

$$\mu = \frac{1}{F^{*2}} - \frac{1}{F^2}.$$

It admits solitary wave solutions of the form

$$Y = \frac{3\mu}{2E} \left[ \cosh\left(\frac{1}{2}\left(\frac{\mu}{W^*}\right)^{1/2} X\right) \right]^{-2}, \tag{3.20}$$

where  $E$  is the elevation number

$$E = \frac{3}{2H_1^2} \left(1 - \frac{R}{H^2}\right).$$

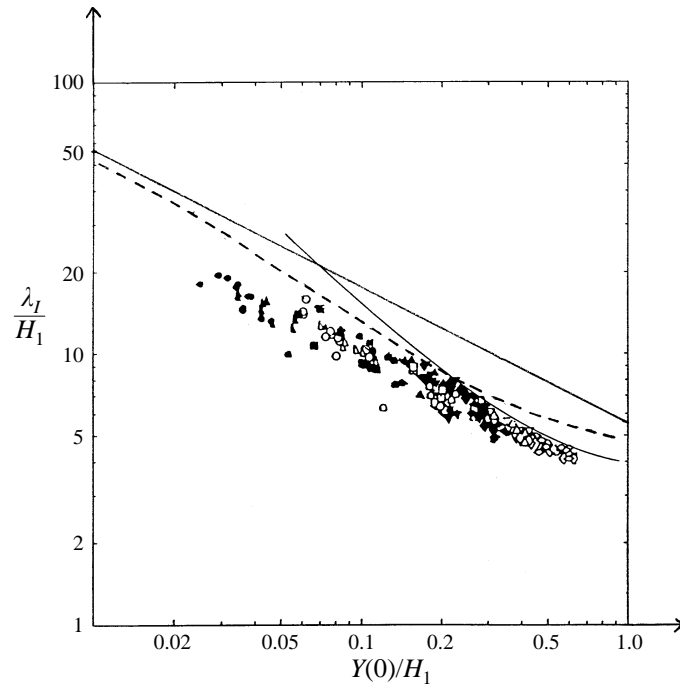


FIGURE 6. Numerical results and comparison with the experiments of Koop & Butler (1981). The parameters are  $R = 0.633$ ,  $H_1 = 0.0277$ ,  $W = 0$ . The straight line represents the results of the Korteweg–de Vries equation. The solid curve represents the results of Choi & Camassa (1996). The dashed line represents the numerical results for the full equations.

Koop & Butler (1981) introduce the quantity

$$\lambda_I = \frac{1}{Y(0)} \int_0^{\infty} Y(X) dX,$$

and plot  $\lambda_I/H_1$  versus  $Y(0)/H_1$ . A straightforward calculation shows that

$$\frac{\lambda_I}{H_1} = \left( \frac{6W^*}{EH_1^3} \right)^{1/2} \left( \frac{Y(0)}{H_1} \right)^{-1/2}.$$

This is shown by the straight line in figure 6. Recently, the experimental results were also compared with the results provided by a model equation derived by Choi & Camassa (1996) and are shown by the solid curve in figure 6. The values of the parameters for the experiments are  $R = 0.633$ ,  $H_1 = 0.0277$ ,  $W = 0$ . The Froude number is allowed to vary. The numerical values obtained with the scheme of § 3.3 are shown by the dashed line in figure 6. The results for the full equations make the link between the results obtained with the KdV equation (small-amplitude waves) and the results obtained with the Choi–Camassa equation (large-amplitude waves). The overall agreement with the experiments is good.

Capillary–gravity solitary waves were computed numerically only for  $W$  larger than the critical value  $W^*$ . Recall that for  $0 < W < W^*$  the solitary waves are generalized. It is easier to describe the global behaviour of the solutions in the  $(H_1, F^2)$ -plane (see figure 7). Like gravity waves, solitary waves bifurcate along the curve  $F = F^*$ . However, for a fixed value of  $H_1$ , the value of the Froude number for the bifurcated wave is smaller than  $F^*$ . When they bifurcate, the solitary waves are of depression if

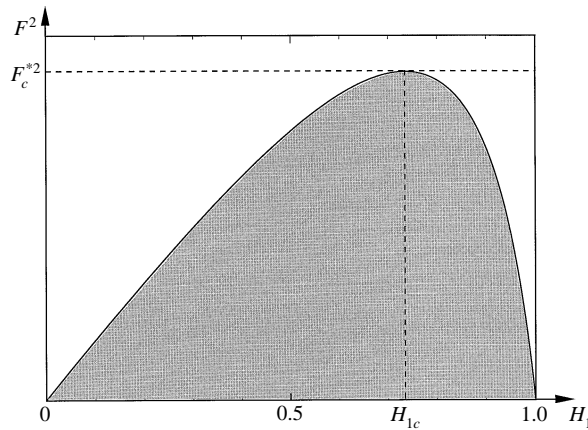


FIGURE 7. Types of solutions in the plane  $F^2$  versus  $H_1$  for  $R = 0.13$  and  $W = 0.5 (> W^*)$ . The curve corresponds to (3.1). Solitary waves are present in the shaded region. They bifurcate along the curve. The bifurcated waves are of depression when  $H_1 < H_{1c}$  and of elevation when  $H_1 > H_{1c}$ . For a fixed value of  $F$  not too far from  $F_c^*$ , the amplitude of the solitary waves of depression increases to the right until the branch reaches the curve again. At that point, the decay of the waves is algebraic. The amplitude of the solitary waves of elevation increases to the left until the branch reaches the curve again. At that point, the decay of the waves is algebraic. Therefore, for any values of  $F^2$  and  $H_1$  inside the shaded region there are both solitary waves of elevation and depression.

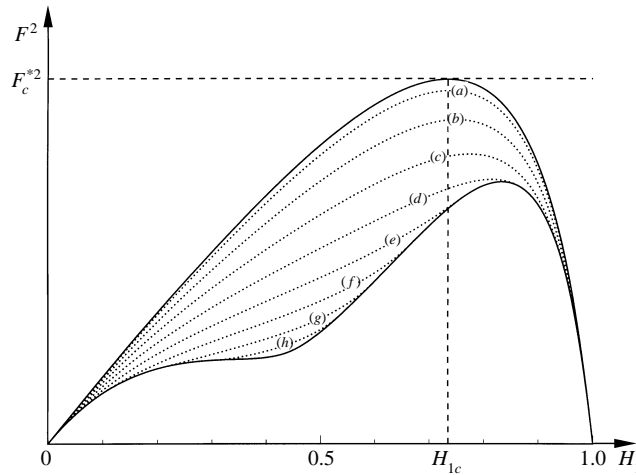


FIGURE 8. Decay rate of capillary-gravity waves at infinity. For  $R = 0.13$  and  $W = 0.5$ , we picked several values for  $\kappa$  in (3.4) ( $\kappa = 0.5$  (a), 1 (b), 1.5 (c), 2 (d), 2.5 (e), 3 (f), 3.5 (g), 4 (h)) and computed the corresponding values of  $F^2(H_1)$ . The lower solid line represents the occurrence of a double root of (3.4). The maximum decay rate, which is  $\kappa = 4.66$ , is obtained for  $F^2 = 0.135$ ,  $H_1 = 0.441$ .

$H_1$  is smaller than the critical value  $H_{1c} = (1 + R^{1/2})^{-1}$  and of elevation if  $H_1 > H_{1c}$ . Let us now pick a value for  $F$  less than  $F_c^*$  and follow the bifurcated waves numerically by increasing  $H_1$  for the depression waves and by decreasing  $H_1$  for the elevation waves. It turns out that these waves can be followed until the curve  $F = F^*$  is reached again. Therefore, for each value of  $F$  and  $H_1$  below the curve, i.e. in the shaded area in figure 7, there are solitary waves of depression and solitary waves of elevation.

Like gravity waves, the bifurcated solitary waves decay exponentially toward infinity. The decay rate is given by the smallest root of (3.4). As the branch of solutions

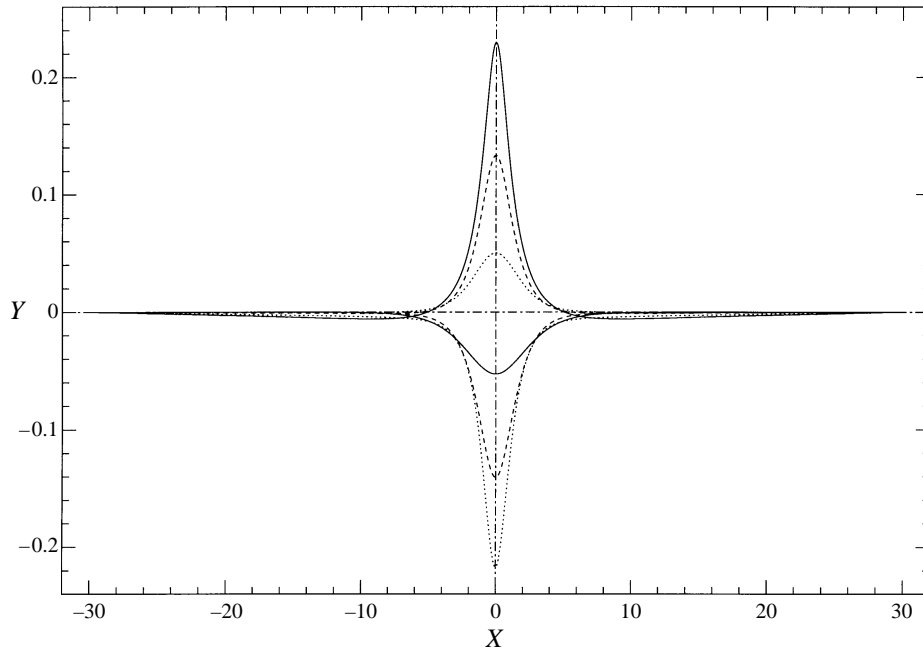


FIGURE 9. Numerical results for capillary-gravity waves, showing the coexistence of depression as well as elevation waves. The parameters are  $R = 0.13$ ,  $F^2 = 0.49$ ,  $W = 0.5$ . The critical values are  $F_c^{*2} = 0.540$ ,  $H_{1c} = 0.735$ . Solitary waves coexist for all values of  $H_1$  between 0.577 and 0.849 (solid line:  $H_1 = 0.63$ , dashed line:  $H_1 = 0.72$ , dotted line:  $H_1 = 0.8$ ).

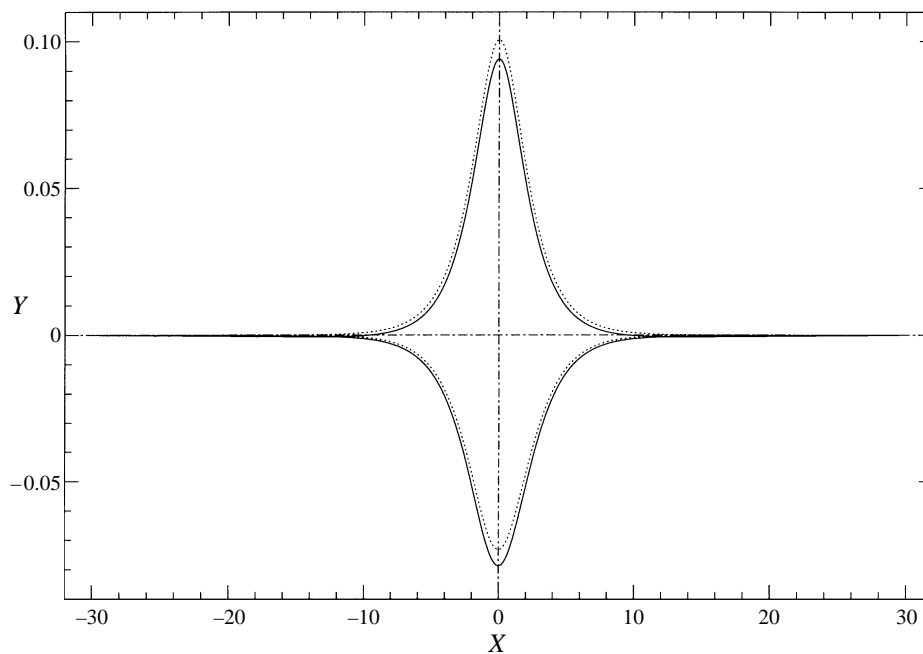


FIGURE 10. Comparison between the numerical results (solid lines) and the results (3.14)–(3.15) from the modified Korteweg-de Vries equation (dotted lines). The parameter values are  $R = 0.13$ ,  $F^2 = 0.52$ ,  $W = 0.5$ ,  $H_1 = 0.72$ .

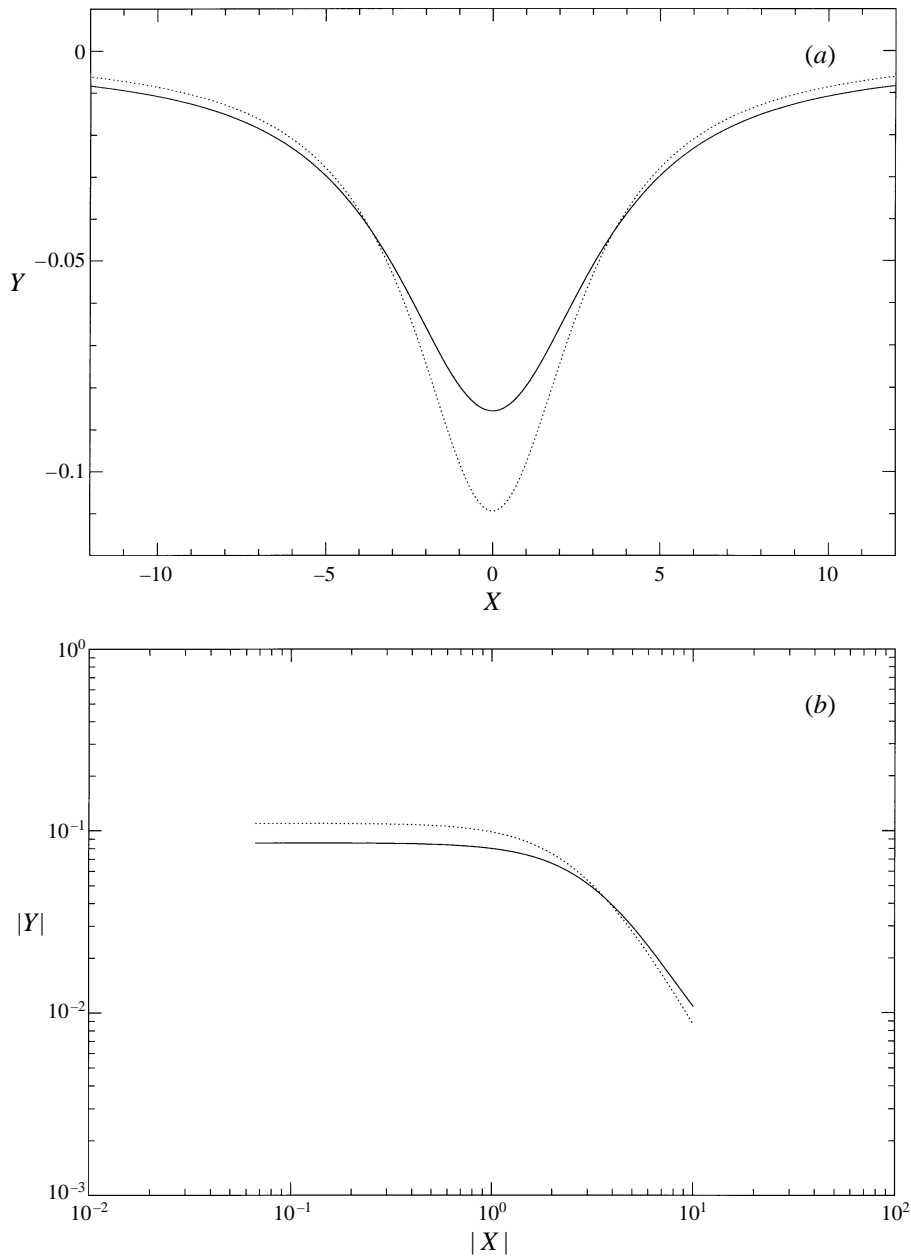


FIGURE 11. Comparison between the numerical result (solid line) and the result (3.12) from the modified Korteweg-de Vries equation (dotted line) for a solitary wave with algebraic decay at infinity. The parameter values are  $R = 0.13$ ,  $F^2 = 0.535$ ,  $W = 0.5$ . The value for  $H_1$  is the largest root of (A 18) ( $H_1 = 0.776$ ). The critical values are  $F_c^{*2} = 0.540$ ,  $H_{1c} = 0.735$ . The profiles are shown in the  $(X, Y)$ -plane: (a) standard scale, (b) logarithmic scale.

reaches the opposite side of the bifurcation curve, the smallest root becomes zero and the decay becomes algebraic, as was already mentioned in §3.4.2 when dealing with the modified Korteweg-de Vries equation. The exponential decay is shown in figure 8. It is possible to have double roots of (3.4). They are indicated on figure 8 as well.

Symbol	Definition	Dimensionless quantity
$K$	$(\sigma/\rho_1 c^2) k$	dimensionless wave number
$R$	$\rho_2/\rho_1$	density ratio
$\alpha$	$\sigma g/(\rho_1 c^4)$	modified Weber number
$X$	$(\rho_1 c^2/\sigma) x$	horizontal coordinate
$Y(X)$	$(\rho_1 c^2/\sigma) \eta$	dimensionless profile of the interface
$(\Phi_j, \Psi_j)$	$(\rho_1 c/\sigma)(\phi_j, \psi_j)$	dimensionless potential and stream function

TABLE 3. Dimensionless quantities

The occurrence of double roots is also indicated in figure 1 by the curve  $\Gamma_2$ . The behaviour of the solutions as the curve  $\Gamma_2$  is crossed is extremely rich. This crossing gives rise to a plethora of solitary waves, which was studied by Buffoni, Groves & Toland (1996) in the context of surface waves. It has not been studied yet in the context of interfacial waves. In the present computations, the parameters were kept inside the region bounded by the bifurcation curve and the curve of double roots in figure 8. A series of profiles is shown in figure 9 for  $F^2 = 0.49$ ,  $R = 0.13$ ,  $W = 0.5$ . The only parameter is  $H_1$ . The spacing is  $\Delta\Phi = 0.075$ , while the number of points is  $N = 400$ . A comparison with the analytical results from the modified KdV equation is given in figure 10 for  $F^2 = 0.52$ ,  $R = 0.13$ ,  $W = 0.5$ ,  $H_1 = 0.72$ .

The algebraically decaying solitary wave solutions of the modified KdV equation decay as  $1/X^2$ . Therefore the corresponding small-amplitude solitary wave solutions of the full Euler equations decay as  $1/X^2$  as well. A comparison is provided in figure 11. However, as one moves away from the critical case  $H^2 \approx R$ , neither the analytical results nor the numerical results allow a precise determination of the exact decay rate at this stage.

## 4. Wave packets

### 4.1. Linear results

The critical parameters for the wavenumber  $K \neq 0$  to be a double root of (2.6) are

$$\frac{1}{F^{*2}} = \frac{K}{2} \left[ \coth(KH_1) + R \coth(KH_2) + \frac{KH_1}{\sinh^2(KH_1)} + R \frac{KH_2}{\sinh^2(KH_2)} \right],$$

$$W^* = \frac{1}{2K} \left[ \coth(KH_1) + R \coth(KH_2) - \frac{KH_1}{\sinh^2(KH_1)} - R \frac{KH_2}{\sinh^2(KH_2)} \right].$$

They are represented by the curve  $\Gamma_1$  in figure 1. For  $R = 0$  and  $H_1 = 1$ , which corresponds to the free-surface problem, we recover the well-known values  $F^*$  and  $W^*$  of Dias & Iooss (1993). From now on, the analysis and the computations are restricted to infinite depth for simplicity's sake. There is no difficulty associated with finite depth except that it is more tedious. Since the total depth was used as unit length above, new dimensionless variables must be introduced. They are shown in table 3. In particular, we introduce the parameter  $\alpha$  obtained by dividing the Weber number by the square of the Froude number:

$$\alpha \equiv \frac{W}{(1-R)F^2}.$$



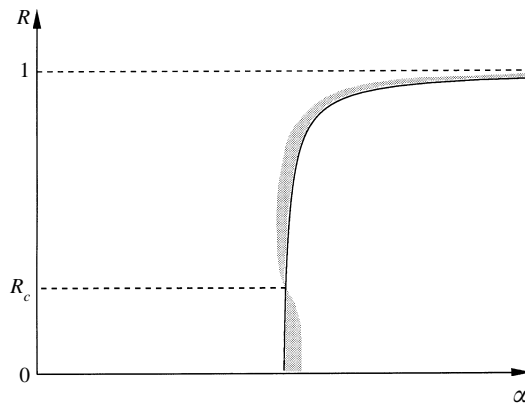


FIGURE 12. Types of solutions in the plane  $R$  versus  $\alpha$  in infinite depth. The curve corresponds to  $\alpha = \alpha^*$  (4.1). Solitary waves in the form of wave packets bifurcate from a train of infinitesimal periodic waves to the right of the curve, when  $R < R_c$ . Dark solitary waves are present to the left of the curve when  $R > R_c$ .

The corresponding values for  $\alpha$  and  $K$  at the critical point are given by

$$\alpha^* = \frac{(1 + R)^2}{4(1 - R)}, \quad K^* = \frac{1 + R}{2}. \tag{4.1}$$

#### 4.2. Nonlinear results

In infinite depth, there is a critical value of the density ratio

$$R_c = (21 - 8\sqrt{5})/11,$$

the origin of which will be made clear in §4.4.1. As shown in figure 12, solutions in the region  $\alpha$  near  $\alpha^*$  are similar to the free-surface problem if  $R < R_c$  (bright solitary waves bifurcate to the right of the curve  $\Gamma_1$ ), while they differ if  $R > R_c$  (dark solitary waves are present to the left of the curve  $\Gamma_1$ ). In this section, we compute bright solitary waves when both fluid layers are infinite. Of course, we compute the solitary waves predicted by the weakly nonlinear analysis but we also show that they exist in the region where the weakly nonlinear analysis predicts only dark solitary waves. The reason is that they exist only at finite amplitude and cannot be captured by a weakly nonlinear analysis.

Before moving to the numerical results, let us recall some facts on the weakly nonlinear results. For a given value of  $\alpha < \alpha^*$  with  $R > R_c$ , there is a one-parameter family of dark solitary waves as shown by Dias & Iooss (1996). This is in contrast with what happens when  $\alpha > \alpha^*$  with  $R < R_c$ . Let us note also that as long as  $R > R_c$  in finite depth, there is always a critical value of the Froude number along the curve  $\Gamma_1$  where the singularity corresponding to the transition bright versus dark solitary waves occurs (see figure 1b) since the fifth-order KdV equation derived in §3.4.3 in the region  $F \approx F^*$ ,  $W \approx W^*$  shows that only bright solitary waves are possible.

#### 4.3. Numerical scheme

The scheme is an extension to two fluid layers of the scheme used by Vanden-Broeck & Dias (1992) for the free-surface problem. Recall that the scaling and dimensionless parameters are given in table 3. As in §3, the interfacial wave problem is solved by a boundary integral equation technique. The complex potentials  $\Phi_j + i\Psi_j$  are introduced

and the interface is described by  $\Psi_j = 0$ . Again, without loss of generality, we choose  $\Phi_j = 0$  at  $X = 0$  on the interface. Let the link between both potentials be again given as

$$\Phi_2 = g(\Phi_1).$$

The potentials have the same asymptotic behaviours as in §3.3. Using Cauchy's integral formula again we get

$$X'_1 = 1 - \frac{1}{\pi} \int_0^{+\infty} Y'_1 \left( \frac{1}{s - \Phi_1} + \frac{1}{s + \Phi_1} \right) ds \quad (4.2)$$

and

$$\frac{X'_1}{g'} = 1 - \frac{1}{\pi} \int_0^{+\infty} Y'_1 \left( \frac{1}{g(s) - g(\Phi_1)} + \frac{1}{g(s) + g(\Phi_1)} \right) ds. \quad (4.3)$$

Bernoulli's equation can be written as

$$\frac{1}{2} \left( \frac{1}{X_1'^2 + Y_1'^2} \right) (1 - Rg'^2) + \alpha(1 - R)Y_1 + \frac{Y_1'X_1'' - X_1'Y_1''}{(X_1'^2 + Y_1'^2)^{3/2}} = \frac{1}{2}(1 - R), \quad (4.4)$$

where the primes denote differentiation with respect to  $\Phi_1$ . The three equations (4.2), (4.3), (4.4) must be solved for the three unknowns  $Y_1$ ,  $g$  and  $X_1$ . The system is discretized by choosing  $N$  points for the potential  $\Phi_1$  with an equal spacing  $\Delta\Phi$  and solved by Newton's method for fixed values of the parameters  $\alpha$  and  $R$ . The handling of the Cauchy principal values is done the same way as in §3.3.

#### 4.4. Analytical solutions

In order to follow the branches of solutions, we start near the bifurcation curves where a good initial guess is provided by the analytical solutions.

The expressions for the steady cubic nonlinear Schrödinger equation and the modified nonlinear Schrödinger equation, which are valid in certain regions of parameter space, are given below. These equations were derived in Dias & Iooss (1996).

##### 4.4.1. Nonlinear Schrödinger equation

Dias & Iooss (1996) showed that, at leading order, the solutions near the curve  $\Gamma_1$  are given by

$$Y(X) = \frac{4}{1 + R} \operatorname{Re} [A(X) e^{iK^*X}],$$

where  $A$  satisfies the cubic nonlinear Schrödinger equation

$$(1 - R)\mu A - A_{XX} - \frac{11 - 42R + 11R^2}{8} A|A|^2 = 0. \quad (4.5)$$

The bifurcation parameter  $\mu$  is defined by

$$\mu = \alpha - \alpha^*.$$

If  $\mu > 0$ , one can introduce the scaling

$$\mu^{1/2} \tilde{A} = A, \quad \tilde{X} = \mu^{1/2} (1 - R)^{1/2} X,$$

and the coefficient

$$C = \frac{11 - 42R + 11R^2}{8(1 - R)}.$$

The coefficient  $C$  vanishes when  $R = R_c$ .

The resulting equation is

$$\tilde{A} - \tilde{A}_{\tilde{X}\tilde{X}} - C\tilde{A}|\tilde{A}|^2 = 0. \tag{4.6}$$

When  $C > 0$ , there are bright solitary waves, the envelope of which is given by

$$\tilde{A} = \pm \frac{\sqrt{2}}{C^{1/2} \cosh \tilde{X}}.$$

In §4.5, we will need  $Y(0)$  for these waves. One finds that

$$Y(0) = \frac{4}{1+R} \left( \frac{2\mu}{C} \right)^{1/2}, \tag{4.7}$$

provided that  $R < R_c$ .

If  $\mu < 0$ , one can introduce the scaling

$$|\mu|^{1/2} \tilde{A} = A, \quad \tilde{X} = |\mu|^{1/2} (1-R)^{1/2} X.$$

The resulting equation is

$$\tilde{A} + \tilde{A}_{\tilde{X}\tilde{X}} + C\tilde{A}|\tilde{A}|^2 = 0.$$

Writing  $\tilde{A} = r(\tilde{X}) e^{i\theta(\tilde{X})}$  leads to

$$r_{\tilde{X}\tilde{X}} + r + Cr^3 - r(\theta_{\tilde{X}})^2 = 0, \tag{4.8}$$

$$2\theta_{\tilde{X}} r_{\tilde{X}} + r\theta_{\tilde{X}\tilde{X}} = 0. \tag{4.9}$$

The system (4.8)–(4.9) has two first integrals  $I_1$  and  $I_2$  defined as follows:

$$u\theta_{\tilde{X}} = I_1, \tag{4.10}$$

$$\frac{1}{4}(u_{\tilde{X}})^2 = -u^2 - \frac{1}{2}Cu^3 - I_1^2 + I_2u, \tag{4.11}$$

where  $u \equiv r^2$ . These two integrals are related to the energy flux and flow force respectively, as shown by Bridges, Christodoulides & Dias (1995). When  $C < 0$ , there is a one-parameter family of dark solitary waves. Let the parameter be  $\gamma_d$ , with  $-2/3C \leq \gamma_d \leq -1/C$ . Then take

$$I_1^2 = C\gamma_d^3 + \gamma_d^2, \quad I_2 = \frac{3}{2}C\gamma_d^2 + 2\gamma_d,$$

in order to have a double root  $\gamma_d$  of the right-hand side of (4.11). The third root  $\gamma_s \leq \gamma_d$  then is

$$\gamma_s = -\frac{2}{C} - 2\gamma_d.$$

The integration of (4.11) provides the envelope of the dark solitary waves:

$$r = \left[ \gamma_s + (\gamma_d - \gamma_s) \tanh^2 \left( \tilde{X} \left( \frac{(\gamma_d - \gamma_s)|C|}{2} \right)^{1/2} \right) \right]^{1/2}. \tag{4.12}$$

Finally,  $\theta(\tilde{X})$  is obtained by integrating (4.10). When  $\gamma_d = -2/3C$ ,  $\gamma_s = \gamma_d$  and the dark solitary wave becomes a periodic wave. When  $\gamma_d = -1/C$ ,  $\gamma_s = 0$  and (4.12) becomes

$$r = |C|^{-1/2} \tanh \left( |\tilde{X}|/\sqrt{2} \right). \tag{4.13}$$

## 4.4.2. Modified nonlinear Schrödinger equation

The unfolding of the singularity  $C = 0$  (or  $R = R_c$ ), which was performed by Dias & Iooss (1996), leads to the modified nonlinear Schrödinger equation

$$A_{XX} - [(1-R)\mu - (1-R)C|A|^2 - (Q - C_1^2 + C_1C_2)|A|^4] A + i [(\frac{1}{2}C_2 - 3C_1)|A|^2 A_X - (\frac{1}{2}C_2 + C_1)A^2 \overline{A}_X] = 0, \quad (4.14)$$

where  $C_1$ ,  $C_2$  and  $Q$  are coefficients depending on  $R$ . Note that the coefficient of the term  $A|A|^4$  should read  $q_4 - p_2^2 + p_2q_3$  in Dias & Iooss (1996) instead of simply  $q_4$ . Solitary wave solutions of (4.14) when  $\mu = 0$  and  $C < 0$  were studied by Iooss (1997). Writing  $A = r(X) e^{i\theta(X)}$  leads to

$$r_{XX} + (1-R)Cr^3 + (Q - C_1^2 + C_1C_2)r^5 - r(\theta_X)^2 + (2C_1 - C_2)r^3\theta_X = 0, \quad (4.15)$$

$$2\theta_X r_X + r\theta_{XX} - 4C_1 r^2 r_X = 0. \quad (4.16)$$

There is a non-trivial solitary wave solution, with algebraic decay at infinity, given by

$$r = \left[ \frac{6|C|(1-R)}{3C^2(1-R)^2 X^2 + 4Q} \right]^{1/2}, \quad (4.17)$$

$$\theta = C_1 \left( \frac{3}{Q} \right)^{1/2} \arctan \left[ \frac{1}{2}|C|(1-R)X \left( \frac{3}{Q} \right)^{1/2} \right]. \quad (4.18)$$

In §4.5, we will need  $Y(0)$  for this solitary wave. One finds that

$$Y(0) = \frac{2}{1+R} \left( \frac{6|C|(1-R)}{Q} \right)^{1/2}, \quad (4.19)$$

provided that  $R > R_c$ . The value of the coefficient  $Q$  evaluated at  $R = R_c$  is 2.76.

## 4.5. Numerical results

As said above, we restricted the numerical computations to infinite depth in both layers and we only computed bright solitary waves. The computation of dark solitary waves is left for future work. In the plane  $R$  versus  $\alpha$  (figure 12), we know from the weakly nonlinear analysis that bright solitary waves bifurcate from infinitesimal periodic waves along the curve  $\alpha = \alpha^*$ , as long as  $R < R_c$ . The main result of this section is that we were able to compute with the numerical scheme described in §4.3 bright solitary waves with damped oscillations in their tail even for values of  $R$  larger than the critical value  $(21 - 8\sqrt{5})/11$ . These waves are always obtained for values of  $\alpha$  larger than  $\alpha^*$ . In figure 13 we follow the evolution of the wave amplitude  $Y(0)$  versus  $\alpha - \alpha^*$ . Figure 13(a) corresponds to a value of  $R$  smaller than the critical value  $R_c$  while figure 13(b) corresponds to a value of  $R$  larger than this critical value. For all values of  $R$ , we can compute both depression and elevations waves. In the case  $R < R_c$ , the results near the bifurcation point  $\alpha = \alpha^*$  are compared with the analytical results (4.7). The main difference between the two cases is that when  $R > R_c$  the solitary waves exist only above a certain amplitude  $Y(0)$ . This phenomenon can also be observed in figure 14 where the evolution of the amplitude  $Y(0)$  is plotted versus  $R$  for  $\mu = 0$ . As long as  $R < R_c$ ,  $Y(0) = 0$ . As  $R$  becomes larger than  $R_c$ , solitary waves of finite amplitude appear at  $\alpha = \alpha^*$ . For values of  $R$  close to  $R_c$ , the numerical results are compared with the results provided by the analytical computations (4.19). The analytical and the numerical results are complementary. Note the behaviour of the elevation branch: it has a limit point at  $R \approx 0.91$ . We computed the second part

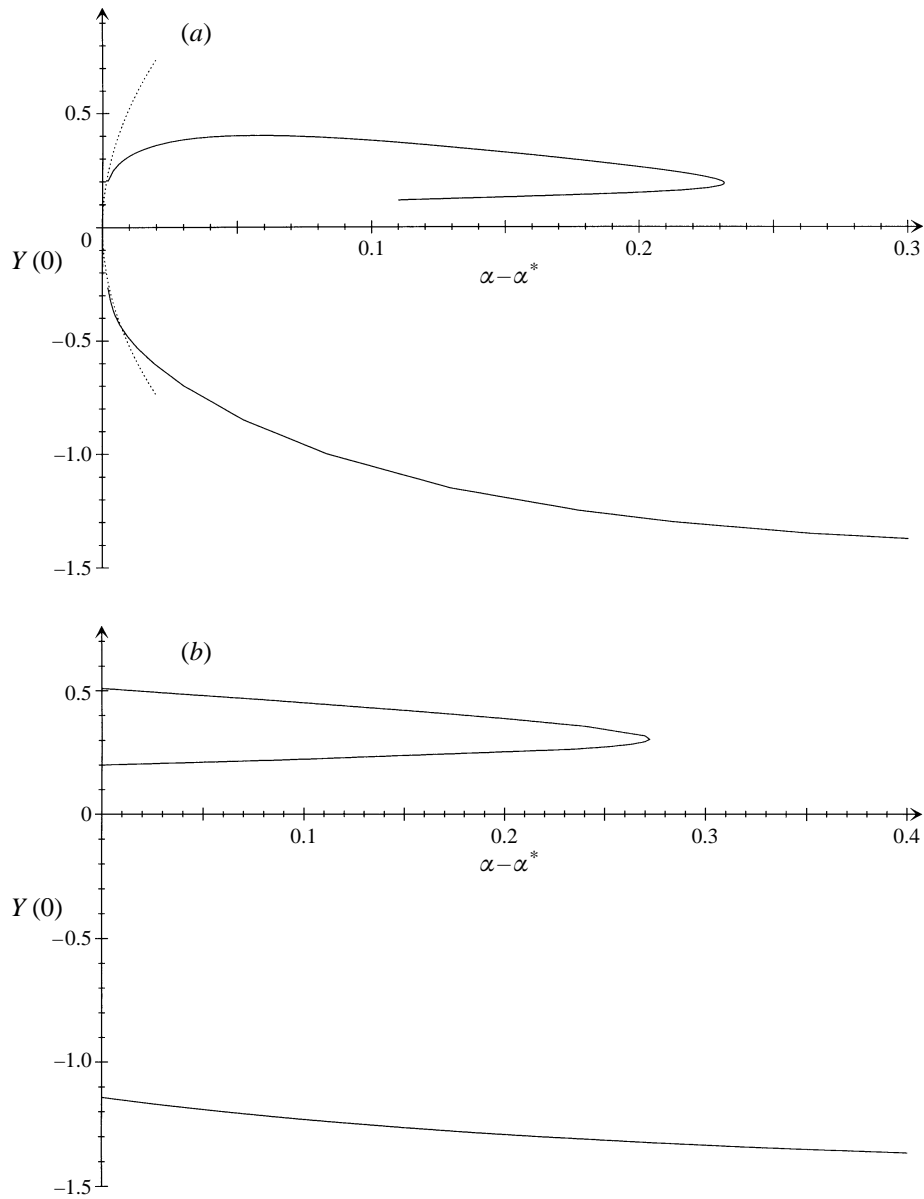


FIGURE 13. Branches of solitary waves in the form of wave packets. The amplitude at the origin is plotted versus  $\alpha - \alpha^*$ . Both the elevation and the depression branches are shown. The elevation branch has a limit point. (a) The density ratio  $R$  is equal to 0.1 and therefore less than the critical ratio  $R_c$ . The value of  $\alpha^*$  is 0.336. The dotted line represents the analytical results given by (4.7). (b) The density ratio  $R$  is equal to 0.7 and therefore greater than the critical ratio  $R_c$ . The value of  $\alpha^*$  is 2.408.

of the branch down to  $R = 0.7$ . It seems that for most values of  $R$  there are at least two branches of elevation waves appearing at  $\alpha = \alpha^*$  (see for example figure 13b for  $R = 0.7$ )! Finally, some computed profiles corresponding to  $R = 0.7$  are shown in figure 15. In all the computations, the spacing is  $\Delta\Phi = 0.1$ , while the number of points is  $N = 900$ . Of course, we did not explore the full structure of the branches

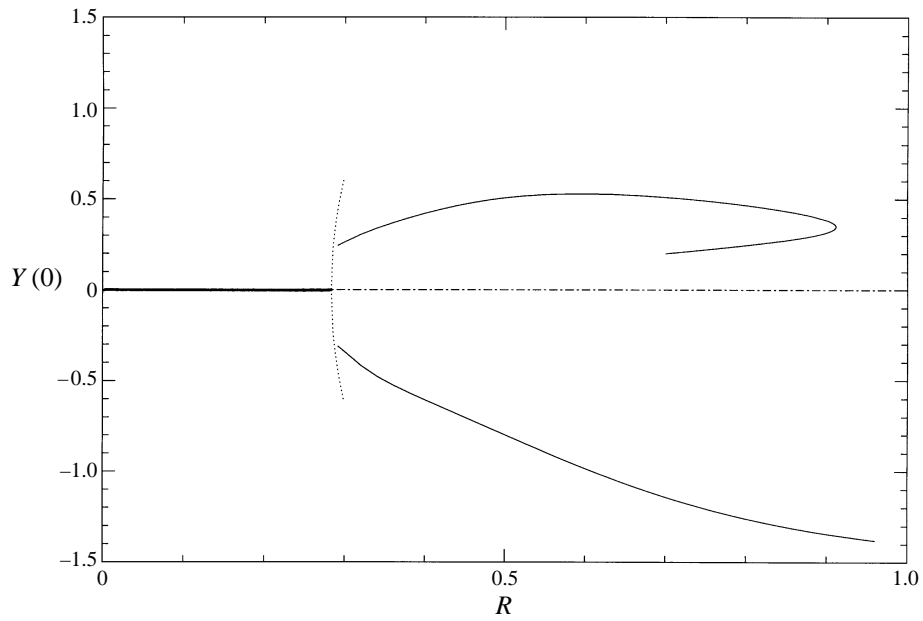


FIGURE 14. Amplitude at the origin of solitary waves when  $\alpha = \alpha^*$ . The dotted line represents the analytical results given by (4.19).

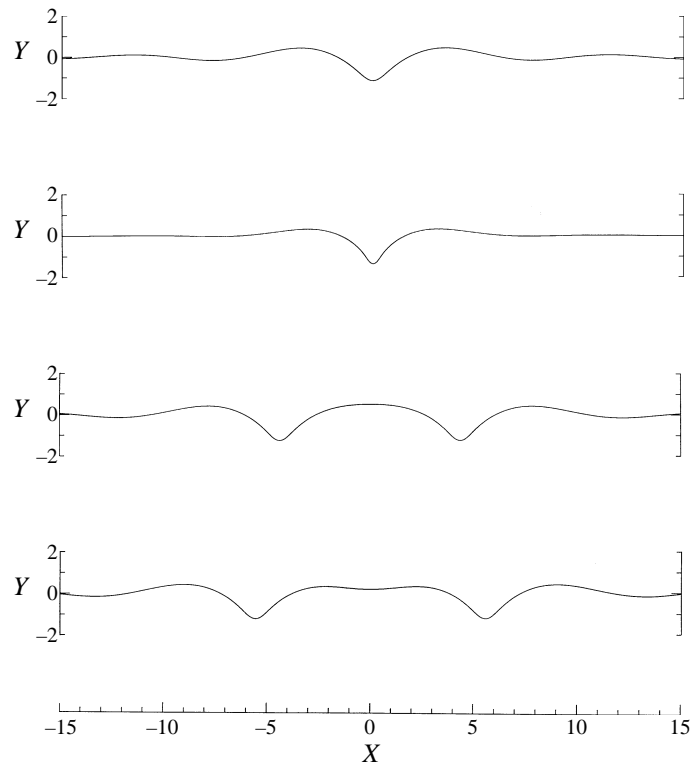


FIGURE 15. Profiles of interfacial solitary waves in the form of wave packets ( $R = 0.7$ ). From top to bottom: depression wave ( $\mu = 0$ ), depression wave ( $\mu = 0.4$ ), elevation wave ( $\mu = 0$ ,  $Y(0) = 0.51$ ), elevation wave ( $\mu = 0$ ,  $Y(0) = 0.20$ ).

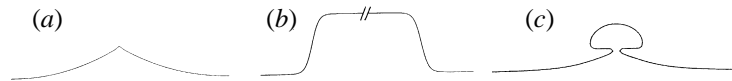


FIGURE 16. Limiting configurations for interfacial gravity waves: (a) surface waves, (b) infinitely broad waves, (c) overhanging waves (from Pullin & Grimshaw 1988, figure 7).

of solutions. Most likely, there is a plethora of solitary waves similar to the plethora encountered in the free-surface case. Note that a high accuracy is required and that the cost of the computations can easily become prohibitive. Recall that with  $N = 900$  there are 1800 nonlinear equations for 1800 unknowns to solve at each iteration!

All the solitary waves in infinite depth with  $\alpha > \alpha^*$  decay like  $1/X^2$  at infinity. This somewhat surprising result (since the solutions of (4.6) feature oscillatory tails with exponentially decaying amplitude) is due to the induced mean flow that is not accounted for in the cubic nonlinear Schrödinger equation (see Akylas, Dias & Grimshaw 1997).

## 5. Discussion

One of the open problems concerning gravity interfacial solitary waves is their limiting configuration. As the velocity increases for a fixed ratio of fluid depths, the waves reach a limiting configuration, which for surface waves ( $R = 0$ ) is a wave with a  $120^\circ$  angle crest (see figure 16a), and for interfacial waves is either an infinitely broad wave (see figure 16b) or a wave with an overhanging region (see figure 16c). To our knowledge, the question of which limiting configuration occurs is an open problem. Numerical evidence has been given for both types of configurations (see for example Pullin & Grimshaw (1988) or Sha & Vanden-Broeck (1993) for overhanging waves and Funakoshi & Oikawa (1986) or Turner & Vanden-Broeck (1988) for very broad waves). For very small or very large  $H$ , the limiting configuration seems to be the overhanging wave. For  $H$  of order one, the limiting configuration seems to be the infinitely broad wave. Note that Amick & Turner (1986) provided global results on gravity interfacial waves. Their analytical results predict either the broadening or the overhanging but cannot predict which one will occur! We performed a lot of numerical computations but could not reach any conclusion because of a lack of precision. To our knowledge, the limiting configuration of capillary-gravity interfacial waves has not been studied yet.

There are theorems available on the symmetry of gravity interfacial solitary waves with respect to the vertical axis and on the fact that the waves never cross the  $X$ -axis (either  $Y(X) > 0$  for all  $X$  or  $Y(X) < 0$  for all  $X$ ). See for example Craig & Sternberg (1991), Li (1991), Maia (1997). For capillary-gravity waves, there are no theorems available but it is likely that one can find capillary-gravity interfacial waves crossing the  $X$ -axis. For example, the sign of  $Y(X)$  of the largest elevation wave in figure 9 is not constant.

As said in the Introduction, experiments on gravity solitary interfacial waves have been reported in the literature, by Koop & Butler (1981) and Michallet & Barthélémy (1996) for example. Evans & Ford (1996) compared the numerical results obtained on the full equations with various observed properties of oceanic internal waves as reported from the Andaman Sea.

Experiments on capillary-gravity interfacial waves have also been reported, especially when there is a relative motion between the two fluids. For example, Pouliquen *et al.* (1992) performed the Reynolds experiment which consists of tilting a tube filled

---

	$\rho_1$	$\rho_2$	$\sigma$	$h_1$	$h_2$	$c$	$c_d$	$L$
unit	$\text{g cm}^{-3}$	$\text{g cm}^{-3}$	$\text{N m}^{-1}$	cm	cm	$\text{cm s}^{-1}$	$\text{cm s}^{-1}$	cm
	1.	0.92	0.08	1.8	1.7	8.3	9.1	6.3

---

TABLE 4. Fluids that could be used for experiments. The lower fluid is water and the upper fluid is an equal mixture of silicone oil v2 and 1-2-3-4-tetrahydronaphtalene. We have indicated the conditions for  $H^2 = R$ ,  $F = F_c^*$ ,  $W = W_c^*$ , i.e. the conditions for the codimension-3 singularity mentioned in §3.4.4. We have also indicated the conditions (speed  $c_d$  and wavelength  $L$ ) for the bright solitary waves at  $\alpha = \alpha^*$  or for the dark solitary waves.

---

with two immiscible fluids, thus creating a shear flow. Of course the purpose of the experiment is not directly related to the present study, but it is interesting to note that an inviscid theory seems to be appropriate to describe the waves they observe. For the fluids used in their experiments, the critical speeds for the ‘classical’ solitary waves near the codimension-3 singularity ( $F = F^*$ ,  $W = W^*$ ,  $H^2 = R$ ) as well as for the bright solitary waves at  $\alpha = \alpha^*$  are shown in table 4. These are ‘realistic’ speeds. The wavelength of the oscillations for the dark solitary waves is also realistic.

Another set of experiments was reported by Zeybeck & Yortsos (1992). They considered the parallel flow of two immiscible fluids in a Hele-Shaw cell and showed that the fluid interfaces could support wave motion which is governed by the KdV equation.

In experiments, viscosity and surfactants can play an important role. Viscous dissipation can be incorporated in the equations for the wave propagation. However, in the Hele-Shaw context, viscous shear is not relevant to long waves.

The discussion above indicates that experiments can probably be done to study some of the interfacial capillary-gravity waves described in this paper. Like water waves, there are difficulties associated with experimental capillary-gravity waves (accurate measure of the surface tension coefficient, dissipation due to viscosity and contamination of the free surface). Solitary waves in the form of wave packets have been observed experimentally by Zhang (1995) in the context of water waves. Benjamin (1992) made some comments on the stability of such waves in the context of interfacial waves. A stability analysis of the ‘classical’ capillary-gravity solitary waves described in §3 might indicate which one of the depression or of the elevation wave is more likely to be observed.

The authors wish to thank Dr Pius Kirrmann for fruitful discussions on the analysis based on centre-manifold reduction. They also wish to thank the referees for the improvements arising from their careful reports. The computations presented in this work were performed on the CRAY C90 vector supercomputer located at IDRIS (Institut du Développement et des Ressources en Informatique Scientifique – France), and were funded by CNRS (Centre National de la Recherche Scientifique).

## Appendix A. Conjugate flows

We consider the occurrence of fronts at the interface between two finite layers of fluid. We suppose that there is a uniform flow upstream and a uniform flow downstream, possibly with different properties. The properties of the flow downstream are denoted with primes. In this Appendix, we show that, for a given density ratio  $R$ ,



all fronts have the same speed upstream

$$c^2 = g(h_1 + h_2) \left( \frac{1 - R^{1/2}}{1 + R^{1/2}} \right), \tag{A 1}$$

and the same depth ratio downstream

$$H'_1 = H_{1c} = \frac{1}{1 + R^{1/2}}. \tag{A 2}$$

The interest here is not in the shape of the interface, just in the upstream and downstream states. Upstream, the velocity  $c$  is the same in the lower and upper layers. The layers have depths  $h_1$  and  $h_2$ . The bottom is located at  $y = 0$ . The results of this Appendix are not new, except perhaps for the remark (A 19) (see for example the Appendix of Funakoshi & Oikawa 1986). The treatment presented here, which is slightly different, can be easily extended to the case of free-surface boundary conditions.

We suppose that all quantities are known upstream. We show that in addition to the trivial solution  $(c'_1, h'_1, c'_2, h'_2) = (c, h_1, c, h_2)$  there are other uniform solutions downstream, provided that the uniform velocity upstream is equal to (A 1). Note that only the special case where both fluids have the same velocity upstream is considered.

We now review the equations one can write, in addition of course to the constraint  $h'_1 + h'_2 = h_1 + h_2$ .

The conservation of mass in both layers gives

$$c'_i h'_i = c h_i, \quad i = 1, 2. \tag{A 3}$$

Next we write down the conservation of momentum. The pressure is assumed to be zero at the interface upstream. Bernoulli's equation gives

$$\frac{1}{2}c^2 + g y + \frac{p_i}{\rho_i} = \frac{1}{2}c^2 + g h_i, \quad i = 1, 2. \tag{A 4}$$

It follows that the momentum upstream is equal to

$$\rho_1 h_1 c^2 + \rho_2 h_2 c^2 + \frac{1}{2} \rho_1 g h_1^2 - \frac{1}{2} \rho_2 g h_2^2. \tag{A 5}$$

Downstream, Bernoulli's equation gives

$$\frac{1}{2}c_i'^2 + g y + \frac{p'_i}{\rho_i} = \frac{1}{2}c^2 + g h_i, \quad i = 1, 2. \tag{A 6}$$

It follows that the momentum downstream is equal to

$$\begin{aligned} & \rho_1 h'_1 c_1'^2 + \rho_2 h'_2 c_2'^2 \\ & + \rho_1 \int_0^{h'_1} \left[ \frac{1}{2}(c^2 - c_1'^2) + g(h_1 - y) \right] dy + \rho_2 \int_{h'_1}^{h_1+h_2} \left[ \frac{1}{2}(c^2 - c_2'^2) + g(h_1 - y) \right] dy. \end{aligned}$$

After computing the integrals and setting the momentum on the left and the momentum on the right equal, one obtains

$$\rho_1 h_1 c^2 + \rho_2 h_2 c^2 = \frac{1}{2} \rho_1 h'_1 (c^2 + c_1'^2) + \frac{1}{2} \rho_2 h'_2 (c^2 + c_2'^2) + \frac{1}{2} g (h_1 - h'_1)^2 (\rho_2 - \rho_1). \tag{A 7}$$

Finally, we write the conservation of energy. The pressure is required to be continuous across the interface. It follows that downstream one has

$$\frac{1}{2} \rho_1 (c^2 - c_1'^2) + g (h_1 - h'_1) (\rho_1 - \rho_2) = \frac{1}{2} \rho_2 (c^2 - c_2'^2). \tag{A 8}$$

Let us now look for non-trivial solutions of equations (A 3), (A 7) and (A 8). There are four unknowns ( $c'_1, h'_1, c'_2, h'_2$ ) for four equations. However, there is also the constraint  $h'_1 + h'_2 = h_1 + h_2$ . Therefore in general we expect the downstream state to be the same as the upstream state, unless some degeneracy condition is satisfied. Let us now find this degeneracy condition. The equations are rewritten in dimensionless form. Equation (A 8) can be written as

$$\frac{1}{F^2} - \frac{H_1 + H'_1}{2H_1'^2} = R \frac{2 - H_1 - H'_1}{2(1 - H_1')^2}, \quad (\text{A } 9)$$

or

$$2F^{-2}H_1'^4 + (R - 1 - 4F^{-2})H_1'^3 + (2F^{-2} + 2 - H_1 + RH_1 - 2R)H_1'^2 + (2H_1 - 1)H_1' - H_1 = 0. \quad (\text{A } 10)$$

Equation (A 7) can be written as

$$\frac{1}{H_1'} + \frac{R}{1 - H_1'} = \frac{1}{F^2}, \quad (\text{A } 11)$$

or

$$F^{-2}H_1'^2 + (R - F^{-2} - 1)H_1' + 1 = 0. \quad (\text{A } 12)$$

Equation (A 10) is in  $H_1'^4$  while (A 12) is in  $H_1'^2$ . Requiring both to have a common root leads to the condition

$$[F^{-2}H_1(H_1 - 1) - H_1 + 1 + RH_1] [1 - 2F^{-2}R - 2F^{-2} - 2R + R^2 + F^{-4}] = 0. \quad (\text{A } 13)$$

Therefore, either

$$\frac{1}{F^2} = \frac{1 - H_1 + RH_1}{H_1(1 - H_1)}, \quad (\text{A } 14)$$

which is the critical speed, or

$$F^{-4} - 2(1 + R)F^{-2} + (1 - R)^2 = 0, \quad (\text{A } 15)$$

that is to say

$$\frac{1}{F} = 1 \pm R^{1/2}.$$

We take the plus sign, since (A 11) clearly shows that  $F$  must be smaller than 1. Therefore

$$F = (1 + R^{1/2})^{-1}. \quad (\text{A } 16)$$

The common root is given by

$$H_1' = H_{1c} = \frac{1}{1 + R^{1/2}}. \quad (\text{A } 17)$$

Now recall that the critical speed for interfacial waves is given by

$$\frac{1}{F^{*2}} = \frac{1}{H_1} + \frac{R}{1 - H_1}. \quad (\text{A } 18)$$

A simple calculation shows that

$$\frac{dF^*}{dH_1} = 0 \Rightarrow H_1 = H_{1c}, \quad (\text{A } 19)$$

which precisely means that  $H_1' = H_1$ . At the maximum,  $F^* = H_{1c}$ .

The front profiles shown in figure 2 have been obtained from the modified Korteweg-de Vries equation in the gravity regime:

$$-\mu Y + W_c^* Y_{XX} + \frac{3}{2H_{1c}^2} \left(1 - \frac{R}{H^2}\right) Y^2 - \frac{2}{H_{1c}^4 H_c} Y^3 = 0,$$

where  $\mu = 1/F^{*2} - 1/F^2$ .

Since  $\mu > 0$ , one can introduce the change of variables

$$\mu^{1/2} \tilde{Y} = \frac{1}{H_{1c}^2} \left(\frac{2}{H_c}\right)^{1/2} Y, \quad \tilde{X} = \mu^{1/2} (W_c^*)^{-1/2} X,$$

and define the coefficient  $Q$  as

$$Q = \frac{3}{2} \left(\frac{H_c}{2\mu}\right)^{1/2} \left(1 - \frac{R}{H^2}\right).$$

The resulting equation is

$$-\tilde{Y} + \tilde{Y}_{\tilde{X}\tilde{X}} + Q\tilde{Y}^2 - \tilde{Y}^3 = 0, \tag{A 20}$$

which is valid if the difference  $|H^2 - R|$  is of the order of  $\mu^{1/2}$ . When  $Q = \pm 3/\sqrt{2}$ , this equation admits solutions in the form of fronts

$$\tilde{Y} = \pm \frac{\sqrt{2}}{1 + e^{-\tilde{X}}} = \pm \frac{1}{\sqrt{2}} \left(1 + \tanh \frac{1}{2}\tilde{X}\right). \tag{A 21}$$

**Appendix B. Derivation of the model equations**

The model equations can be obtained by using classical perturbation expansions. An alternative way is to use centre-manifold reduction after rewriting the equations (2.1)–(2.5) as a dynamical system in space,  $X$  being the evolution variable. Kirrmann (1991) and Mielke (1995) used this approach to reduce the problem of interfacial waves to a set of ordinary differential equations. We define dimensionless velocity components as

$$U_i = 1 - \frac{c}{u_i}, \quad V_i = \frac{v_i}{u_i}, \quad i = 1, 2. \tag{B 1}$$

We take  $X$  and  $\Psi$  as the new independent variables. The resulting dynamical system formulation of the problem is

$$U_{jX} = -V_{j\Psi} \quad (j = 1, 2), \tag{B 2a}$$

$$V_{jX} = U_{j\Psi} + \frac{2V_j}{1 - U_j} V_{j\Psi} + \frac{V_j^2 - U_j^2 + 2U_j}{(1 - U_j)^2} U_{j\Psi} \quad (j = 1, 2), \tag{B 2b}$$

$$Y_{XX} = \frac{(1 + Y_X^2)^{3/2}}{W} \left[ \frac{1}{F^2} Y + \frac{V_1^2 - U_1^2 + 2U_1}{2(1 - U_1)^2} - R \frac{V_2^2 - U_2^2 + 2U_2}{2(1 - U_2)^2} \right], \tag{B 2c}$$

with the boundary conditions

$$V_1(\cdot, 0) = V_2(\cdot, 0) = Y_X.$$

In Bernoulli's equation,  $Y$  can be eliminated by integrating (B 2a) with respect to  $\Psi$  and then with respect to  $X$ :

$$Y = - \int_{-H_1}^0 U_1 d\Psi + \mathcal{C}_1 \quad \text{and} \quad Y = \int_0^{H_2} U_2 d\Psi + \mathcal{C}_2.$$

Usually, one takes both constants to be zero from mass conservation arguments. Therefore

$$\int_{-H_1}^0 U_1 d\Psi + \int_0^{H_2} U_2 d\Psi = 0. \quad (\text{B } 3)$$

However, we will only take  $\mathcal{C}_1$  to be zero. By doing so, we will introduce a zero eigenvalue in the problem. By keeping both constants arbitrary, we would introduce two zero eigenvalues in the problem. All the consequences of these zero eigenvalues are not fully understood yet.

Let us introduce  $\beta(X) = V_1(X, 0) = V_2(X, 0)$ . From now on,  $Y$  in Bernoulli's equation is replaced by  $-[U_1]$ , where  $[U_1]$  stands for

$$[U_1] = \int_{-H_1}^0 U_1(\Psi) d\Psi.$$

The reduction procedure can be applied close to  $F = F^*$  (3.1) or close to the curve  $\Gamma_1$  (4.1). From now on, the analysis will be restricted to the case when the parameter  $F$  is close to the critical value  $F^*$ . Therefore the bifurcation parameter  $\mu = 1/F^2 - 1/F^{*2}$  is introduced. Introducing the vector  $\mathbf{w} = [\beta, U_1, V_1, U_2, V_2]$ , the system to be solved can be written as

$$\mathbf{w}_X = \mathbf{L}_\mu \mathbf{w} + \mathbf{N}(\mathbf{w}), \quad (\text{B } 4)$$

where  $\mathbf{L}_\mu$  is the linearization about  $\mathbf{w} = 0$  and  $\mathbf{N}$  represents the nonlinear terms. The linear operator  $\mathbf{L}_\mu$  depends on the parameters  $R$  and  $W$ , and acts on  $\mathbf{w}$  as follows:

$$\mathbf{L}_\mu \mathbf{w} = \mathbf{L}_\mu(R, W) \mathbf{w} = \left[ \frac{1}{W} \left( U_1(0) - R U_2(0) - \left( \frac{1}{F^{*2}} + \mu \right) [U_1] \right), -V_1', U_1', -V_2', U_2' \right], \quad (\text{B } 5)$$

with boundary conditions

$$V_1(0) = V_2(0), \quad V_1(-H_1) = V_2(H_2) = 0.$$

The primes represent derivatives with respect to  $\Psi$ .

The quadratic terms in  $\mathbf{N}$  take the form

$$N_2(\mu; R, W) = [f_0(\mu; R, W), 0, f_1(\mu; R, W), 0, f_2(\mu; R, W)],$$

where

$$f_0(\mu; R, W) = \frac{1}{2W} (3U_1^2(0) - 3RU_2^2(0) + V_1^2 - RV_2^2 + \frac{3}{2}\beta^2(1-R)),$$

$$f_j(\mu; R, W) = 2V_j V_j' + 2U_j U_j' + V_j U_j' \quad (j = 1, 2).$$

The linearization of the equations about the rest state  $\mathbf{w} = 0$  gives

$$\mathbf{w}_X = \mathbf{L}_\mu \mathbf{w}.$$

The non-zero eigenvalues  $\lambda$  of  $\mathbf{L}_\mu$  satisfy the relation

$$\frac{1}{F^2} - W \lambda^2 = \lambda \left[ \frac{R}{\tan(\lambda H_2)} + \frac{1}{\tan(\lambda H_1)} \right]. \quad (\text{B } 6)$$

When  $\lambda$  is purely imaginary, one recovers the dispersion relation (2.6) while when  $\lambda$  is real, one recovers the equation (3.4) for the decay rate.

Zero is always an eigenvalue. Its eigenvector is given by

$$\boldsymbol{\varphi}_0 = \left[ 0, -1, 0, \frac{H_1/F^2 - 1}{R}, 0 \right],$$

which, when  $\mu = 0$ , takes the form

$$\boldsymbol{\varphi}_0 = \left[ 0, -1, 0, \frac{1}{H}, 0 \right].$$

This zero eigenvalue could be eliminated by requiring the velocities  $U_1$  and  $U_2$  to approach zero at infinity.

When  $\mu = 0$ , zero is a triple eigenvalue. The extra eigenvectors are given by

$$\boldsymbol{\varphi}_1 = \begin{pmatrix} H_1 \\ 0 \\ \Psi + H_1 \\ 0 \\ -(1/H)(\Psi - H_2) \end{pmatrix}, \quad \boldsymbol{\varphi}_2 = \begin{pmatrix} 0 \\ \frac{1}{2}\Psi^2 + H_1\Psi + \frac{1}{3}H_1^2 \\ 0 \\ -(1/H) \left[ \frac{1}{2}\Psi^2 - H_2\Psi + (H_2/R)(W - \frac{1}{3}H_1) \right] \\ 0 \end{pmatrix}.$$

We define the scalar product

$$\langle (\beta, U_1, V_1, U_2, V_2), (\tilde{\beta}, \tilde{U}_1, \tilde{V}_1, \tilde{U}_2, \tilde{V}_2) \rangle = \beta\tilde{\beta} + \int_{-H_1}^0 (U_1\tilde{U}_1 + V_1\tilde{V}_1)d\Psi + \int_0^{H_2} (U_2\tilde{U}_2 + V_2\tilde{V}_2)d\Psi.$$

The adjoint operator is given by

$$L_\mu^* \boldsymbol{w} = L_\mu^*(R, W)\boldsymbol{w} = \left[ -U_1(0) + U_2(0), -V_1' + \left( \frac{1}{F^{*2}} + \mu \right) V_1(0), U_1', -V_2', U_2' \right],$$

with boundary conditions

$$V_1(0) = -\frac{\beta}{W}, \quad V_2(0) = -R\frac{\beta}{W}, \quad V_1(-H_1) = V_2(H_2) = 0.$$

The primes represent derivatives with respect to  $\Psi$ .

Zero is always an eigenvalue with eigenvector

$$\boldsymbol{\psi}_2 = [0, 1, 0, 1, 0].$$

When  $\mu = 0$ , the two extra eigenvectors are

$$\boldsymbol{\psi}_1 = \begin{pmatrix} -(W/R)H_2 \\ 0 \\ (1/R)H\Psi + (1/R)H_2 \\ 0 \\ -\Psi + H_2 \end{pmatrix} \quad \text{and} \quad \boldsymbol{\psi}_0 = \begin{pmatrix} 0 \\ (1/2R)H\Psi^2 + (1/R)HH_1\Psi \\ 0 \\ -\frac{1}{2}\Psi^2 + H_2\Psi - (W/R)H_2 \\ 0 \end{pmatrix}.$$

Let  $\boldsymbol{\psi}'_i (i = 0, 1, 2)$  denote the normalized eigenvectors, which are such that  $\langle \boldsymbol{\varphi}_i, \boldsymbol{\psi}'_j \rangle = \delta_{ij}$ . One has

$$\begin{aligned} \boldsymbol{\psi}'_2 &= \mathcal{C}^{-1} \boldsymbol{\psi}_2, \\ \boldsymbol{\psi}'_1 &= \mathcal{C}^{-1} \boldsymbol{\psi}_1, \\ \boldsymbol{\psi}'_0 &= \mathcal{C}^{-1} (\boldsymbol{\psi}_0 - (\mathcal{A}/\mathcal{C})\boldsymbol{\psi}_2), \end{aligned}$$

where

$$\mathcal{A} = H_1 H_2 \left[ \frac{2}{15} H_2^3 - \frac{2W}{3R} H_2^2 + \frac{1}{9R} H_1 H_2^2 + \frac{1}{45R} H_1^3 + \frac{W}{R^2} \left( W - \frac{1}{3} H_1 \right) H_2 \right],$$

$$\mathcal{C} = (W^* - W) \frac{H_1 H_2}{R}.$$

We now write  $w$  in terms of  $\varphi_0$ ,  $\varphi_1$  and  $\varphi_2$ :

$$w = a_0(X)\varphi_0 + a_1(X)\varphi_1 + a_2(X)\varphi_2 + \dots$$

At leading order, the amplitudes  $a_0$  and  $a_1$  satisfy the system

$$a_{0X} = a_1, \quad a_{1X} = \mu P_{11} a_0 + P_{02} a_0^2, \quad (\text{B } 7)$$

where

$$P_{11} = \frac{1}{W - W^*} \quad \text{and} \quad P_{02} = -\frac{3H_2}{2R\mathcal{C}} \left( 1 - \frac{R}{H^2} \right).$$

The coefficient  $P_{11}$  is easy to obtain from the relation (B 6). The coefficient  $P_{02}$  is given by

$$P_{02} = \langle N_2(\varphi_0, \varphi_0), \psi'_1 \rangle.$$

At leading order, one obtains

$$Y_X = \beta, \quad \beta = H_1 a_1 + \dots, \quad Y = H_1 a_0 + \dots$$

and therefore

$$\mu Y + (W^* - W) Y_{XX} + \frac{3}{2H_1^2} \left( 1 - \frac{R}{H^2} \right) Y^2 = 0, \quad (\text{B } 8)$$

which is precisely (3.8).

The modified as well as the fifth-order Korteweg–de Vries equations can be obtained by using the same reduction method.

#### REFERENCES

- AKYLAS, T. R., DIAS, F. & GRIMSHAW, R. H. J. 1997 The effect of the induced mean flow on solitary waves in deep water. *J. Fluid Mech.* (submitted).
- AMICK, C. J. & TURNER, R. E. L. 1986 A global theory of internal solitary waves in two-fluid systems. *Trans. Am. Math. Soc.* **298**, 431–484.
- AMICK, C. J. & TURNER, R. E. L. 1989 Small internal waves in two-fluid systems. *Arch. Rat. Mech. Anal.* **108**, 111–139.
- BENJAMIN, T. B. 1992 A new kind of solitary wave. *J. Fluid Mech.* **245**, 401–411.
- BENJAMIN, T. B. 1996 Solitary and periodic waves of a new kind. *Phil. Trans. R. Soc. Lond. A* **354**, 1775–1806.
- BRIDGES, T. J., CHRISTODOULIDES, P. & DIAS, F. 1995 Spatial bifurcations of interfacial waves when the phase and group velocities are nearly equal. *J. Fluid Mech.* **285**, 121–158.
- BUFFONI, B., GROVES, M. D. & TOLAND, J. F. 1996 A plethora of solitary gravity–capillary water waves with nearly critical Bond and Froude numbers. *Phil. Trans. R. Soc. Lond. A* **354**, 575–607.
- CHOI, W. & CAMASSA, R. 1996 Long internal waves of finite amplitude. *Phys. Rev. Lett.* **77**, 1759–1762.
- CRAIG, W. & STERNBERG, P. 1991 Comparison principles for free-surface flows with gravity. *J. Fluid Mech.* **230**, 231–243.
- DIAS, F. & IOOSS, G. 1993 Capillary–gravity solitary waves with damped oscillations. *Physica D* **65**, 399–423.

- DIAS, F. & IOOSS, G. 1994 Ondes solitaires "noires" à l'interface entre deux fluides en présence de tension superficielle. *C. R. Acad. Sci. Paris* **319** I, 89–93.
- DIAS, F. & IOOSS, G. 1996 Capillary-gravity interfacial waves in deep water. *Eur. J. Mech. B* **15**, 367–393.
- DIAS, F., MENASCE, D. & VANDEN-BROECK, J.-M. 1996 Numerical study of capillary-gravity solitary waves. *Eur. J. Mech. B* **15**, 17–36.
- EVANS, W. A. B. & FORD, M. J. 1996 An integral equation approach to internal (2-layer) solitary waves. *Phys. Fluids* **8**, 2032–2047.
- FUNAKOSHI, M. & OIKAWA, M. 1986 Long internal waves of large amplitude in a two-layer fluid. *J. Phys. Soc. Japan* **55**, 128–144.
- IOOSS, G. 1997 Existence d'orbites homoclines à un équilibre elliptique, pour un système réversible. *C. R. Acad. Sci. Paris* **324** I, 993–997.
- IOOSS, G. & KIRCHGÄSSNER, K. 1990 Bifurcation d'ondes solitaires en présence d'une faible tension superficielle. *C. R. Acad. Sci. Paris* **311** I, 265–268.
- IOOSS, G. & KIRRMANN, P. 1996 Capillary gravity waves on the free surface of an inviscid fluid of infinite depth. Existence of solitary waves. *Arch. Rat. Mech. Anal.* **136**, 1–19.
- KIRRMANN, P. 1991 Reduktion nichtlinearer elliptischer Systeme in Zylindergebieten unter Verwendung von optimaler Regularität in Hölder-Räumen. PhD Thesis, Universität Stuttgart.
- KOOP, C. G. & BUTLER, G. 1981 An investigation of internal solitary waves in a two-fluid system. *J. Fluid Mech.* **112**, 225–251.
- LI, C. 1991 Monotonicity and symmetry of solutions of fully nonlinear elliptic equations on unbounded domains. *Commun. Partial Diff. Equat.* **16**, 585–615.
- MAIA, L. A. 1997 Symmetry of internal waves. *Nonlinear Analysis, Theor., Meth. Appl.* **28**, 87–102.
- MICHALLET, H. & BARTHÉLÉMY, E. 1996 Validation expérimentale de théories asymptotiques pour l'étude des ondes solitaires interfaciales. *C. R. Acad. Sci. Paris* **322** IIb, 541–544.
- MIELKE, A. 1995 Homoclinic and heteroclinic solutions in two-phase flow. *Proc. IUTAM/ISIMM Symp. on Structure and Dynamics of Nonlinear Waves in Fluids*, pp. 353–362. World Scientific.
- MIRIE, R. M. & PENNELL, S. A. 1989 Internal solitary waves in a two-fluid system. *Phys. Fluids A* **1**, 986–991.
- MONI, J. N. & KING, A. C. 1995 Guided and unguided interfacial solitary waves. *Q. J. Mech. Appl. Maths* **48**, 21–38.
- POULIQUEN, O., CHOMAZ, J.-M., HUERRE, P. & TABELING, P. 1992 Wave-number selection and phase solitons in spatially forced temporal mixing layers. *Phys. Rev. Lett.* **68**, 2596–2599.
- PULLIN, D. I. & GRIMSHAW, R. H. J. 1988 Finite-amplitude solitary waves at the interface between two homogeneous fluids. *Phys. Fluids* **31**, 3550–3559.
- SHA, H. & VANDEN-BROECK, J.-M. 1993 Two-layer flows past a semicircular obstruction. *Phys. Fluids A* **5**, 2661–2668.
- SUN, S. M. & SHEN, M. C. 1993 Solitary waves in a two-layer fluid with surface tension. *SIAM J. Math. Anal.* **24**, 866–891.
- TURNER, R. E. L. & VANDEN-BROECK, J.-M. 1988 Broadening of interfacial solitary waves. *Phys. Fluids* **31**, 2486–2490.
- VANDEN-BROECK, J.-M. & DIAS, F. 1992 Gravity-capillary solitary waves in water of infinite depth and related free surface flows. *J. Fluid Mech.* **240**, 549–557.
- ZEYBEK, M. & YORTSOS, Y. C. 1992 Parallel flow in Hele-Shaw cells. *J. Fluid Mech.* **241**, 421–442.
- ZHANG, X. 1995 Capillary-gravity and capillary waves generated in a wind wave tank: observations and theories. *J. Fluid Mech.* **289**, 51–82.